Journal of Catalysis **181,** 124–144 (1999)
Article ID jcat.1998.2293, available online at http://www.idealibrary.com on IDEAL®

DFT Study of the Isomerization of Hexyl Species Involved in the Acid-Catalyzed Conversion of 2-Methyl-Pentene-2

M. A. Natal-Santiago, R. Alcalá, and J. A. Dumesic[1]

Department of Chemical Engineering, University of Wisconsin, Madison, Wisconsin 53706

Received June 23, 1998; revised October 1, 1998; accepted October 7, 1998

Quantum-chemical calculations were conducted on the basis of density-functional theory to study reactions of hexyl species involved in the acid-catalyzed isomerization of 2-methyl-pentene-2. The production of 4-methyl-pentene-2 and 3-methyl-pentene-2 involves 1,2-migrations of hydrogen atoms and methyl groups whose activation energies are lower than 30 kJ/mol for gaseous carbenium ions. The activation energy for branching rearrangements of gaseous hexyl cations to form 2,3-dimethyl-butene-2 is 94 kJ/mol. Transformations of hexyl species were studied in the presence of gaseous water and an aluminosilicate site to simulate reactions on acidic oxides. In the presence of these oxygenated (conjugate) bases, the cationic center in the carbenium ions bonds with oxygen to form alkoxonium ions and alkoxy species, respectively. The relative energies of these species are fairly insensitive to their secondary or tertiary nature. Reactive intermediates of the same order are stabilized more than the corresponding transition states upon interaction with an oxygenated base, thus leading to an increase in the activation energies of isomerization reactions. Transition states have greater separation of electronic charge than the corresponding alkoxonium ions and alkoxy species. The transition state for branching rearrangement requires the greatest separation of electronic charge in the aluminosilicate cluster; the transition state for methyl migration requires the second greatest separation of electronic charge; transition states for hydride shifts require a smaller separation of electronic charge; and transition states for the protonation of alkenes to form alkoxy species require the least separation of electronic charge in the aluminosilicate cluster. These observations imply the existence of a correlation between the positive charge localized in the hydrocarbon fragment of a transition state and the sensitivity of the corresponding reaction pathway to changes in the acidity of the catalyst. Lastly, activation energies for alkene isomerization reactions over aluminosilicates are determined by the energies of transition states with respect to the gaseous reactants plus the acid site and not by the relative stabilities of the alkoxy intermediates in the reaction scheme. © 1999 Academic Press

Key Words: **carbenium; alkoxonium; alkoxy; methyl-pentene; isomerization; silica–alumina; density-functional theory (dft).**

1. INTRODUCTION

The acid-catalyzed conversion of hydrocarbons through cracking, alkylation, and isomerization reactions is of importance in the petrochemical industry (1). Catalysts used for these transformations typically consist of inorganic liquid acids (e.g., H_2SO_4) or solid oxides such as amorphous aluminosilicates and zeolites. Mechanisms for acid-catalyzed conversions of hydrocarbons have traditionally been described in terms of carbenium and/or carbonium ions (2–11), which have been observed in homogeneous, superacidic media (12–14). For example, carbenium ions may be formed by protonation of alkenes or by protolytic cracking of alkanes via carbonium ions. These carbenium ions may then lead to surface chain reactions, involving propagation steps such as isomerization, oligomerization, β-scission, and hydride transfer, which are eventually terminated by steps such as desorption of alkenes and formation of coke.

The isomerization of carbenium ions proceeds through branching and nonbranching rearrangements. Nonbranching rearrangements involve successive hydrogen and alkyl migration steps, whose activation energies are typically lower than 30 kJ/mol when the degree of the cation remains constant (as in transitions between secondary carbenium ions) (13, 14). These processes are believed to proceed via transition states containing three-center, two-electron bonds involving the migrating entity. In contrast, activation energies of branching rearrangements of species having more than four carbon atoms are typically higher than 65 kJ/mol (13, 14), and these processes are believed to proceed via transition states that resemble protonated cyclopropane rings.

Activity and selectivity patterns for the conversion of hydrocarbons over solid acid catalysts have been explained using analogies with reactions of carbenium ions in acidic solutions (2–11), where reactivity trends are typically based on differences in the stabilities of primary, secondary, and tertiary carbenium ions. However, this traditional viewpoint has been shown to be overly simplistic, since the reactive intermediates on solid catalysts are more similar

[1] To whom correspondence should be addressed.

0021-9517/99 $30.00

to (neutral) alkoxy species than to (charged) carbenium ions. Despite evidence for the existence of cyclopentenyl, indanyl, and trityl cations on acidic zeolites (15, 16), most spectroscopic (15, 17–23) and quantum-chemical (20, 24–34) investigations have shown that the ground states of protonated species involve strong interactions with surface oxygen atoms (the conjugate basic form of the adsorption site). Therefore, these species are described more correctly as alkoxy species covalently bonded to the oxide surface, and their relative stabilities are insensitive to whether the hydrocarbon fragment is of a primary, secondary, or tertiary nature. However, these alkoxy species may react via formation of transition states that resemble carbenium ions by stretching of the C–O bond (3, 24, 25, 35–44). Because of the ionic character of these transition states, activation energies for reactions of hydrocarbons on solid acid catalysts are different for primary, secondary, and tertiary species, thereby suggesting that the success of kinetic models based on reactions of carbenium ions is caused by an ordering of the activation energies rather than the relative stabilities of the reaction intermediates (25).

Reactions of hydrocarbons that possess multiple pathways are useful probes for the characterization of acid catalysts (45–48). Figure 1 shows several pathways for isomerization of hexyl species in the acid-catalyzed conversion of 2-methyl-pentene-2 (2-MP-2). According to McVicker and coworkers (45, 46, 48), the conversion of 2-MP-2 can be catalyzed by amorphous aluminosilicates and the relative rates of isomerization processes depend on the acidity of the catalyst: weak acids catalyze migration of the double bond to produce 4-methyl-pentene-2 (4-MP-2) via 1,2-hydride shifts; stronger acids are required to catalyze methyl migrations that lead to 3-methyl-pentene-2 (3-MP-2); and even stronger acids are needed to achieve branching rearrangements involved in the production of 2,3-dimethyl-butene-2 (2,3-DMB-2).

In the present paper, we present results from quantum-chemical calculations performed on the basis of density-functional theory (DFT) to study the isomerization of hexyl species involved in the acid-catalyzed conversion of 2-MP-2 to 4-MP-2, 3-MP-2, and 2,3-DMB-2. Our studies consist of three scenarios: isomerization of hexyl cations in the gas phase, reaction in the presence of gaseous water, and transformations of hexyl species on a Brønsted acid site characteristic of amorphous aluminosilicates. The use of a water molecule is intended as a first approximation to simulate the conjugate basic form of an acid site after protonation of an alkene. The use of a neutral $(OH)_3SiOHAl(OH)_3$ cluster is intended to simulate more realistically the acid site of an amorphous aluminosilicate. The three scenarios chosen for our studies provide a general view of how the rates of isomerization of hexyl species are affected as the acidity of the acid site becomes progressively weaker in moving from $H^{\oplus}$ to $H_3O^{\oplus}$ to a neutral aluminosilicate.

Quantum-chemical calculations have been performed previously for the isomerization of gaseous butyl (49–51) and pentyl (52) cations; however, to our knowledge, these calculations have not yet been conducted for the isomerization of hexyl species. We will show that the activation energies for hydride and methyl migrations involving gaseous carbenium ions are lower than 30 kJ/mol. Reactions involving cations of the same degree proceed through transition states that contain two-electron, three-center bonds involving the migratory entity, whereas transition states for reactions involving cations of different degree resemble the less stable, in our case secondary, cations. Activation energies for branching rearrangements in the gas phase are predicted to be near 94 kJ/mol, and these reactions proceed via transition states that resemble protonated cyclopropane rings. In the presence of a water molecule, the cationic centers of the various hexyl cations interact with oxygen to form alkoxonium ions whose relative energies are less sensitive to their degree, that is, whether they are secondary or tertiary species. The relative energies of the various hexyl (alkoxy) species on the aluminosilicate site are even less sensitive to their degree. Hydride and methyl migrations, as well as branching reactions, for these alkoxonium ions and alkoxy species require the separation of electronic charge and proceed through transition states in which the positive charge becomes more localized in the hydrocarbon fragment.

2. METHODOLOGY

Quantum-chemical calculations were performed on the basis of DFT, using the three-parameter functional B3LYP (53) along with gaussian-type basis sets (54). This functional was chosen because it has been shown (52) to describe transformations of hydrocarbons as well as Møller–Plesset perturbation methods (54), while being computationally more efficient. In general, DFT functionals are known to work well for the prediction of thermochemical properties of systems containing light atoms, although they become less useful for the description of heavy atoms or highly charged systems (55).

The basis set 6-31G* was used to study reactions of isolated hexyl cations, while the larger basis set 6-31 + G* was used to compare transformations of carbenium ions in the gas phase and in the presence of a water molecule. Reactions on amorphous aluminosilicates were studied using the Brønsted acid site $(OH)_3SiOHAl(OH)_3$. This cluster was chosen because it is the smallest one that can be used reliably while maintaining an acceptable computational cost. However, it should be recalled that quantum-chemical calculations within the cluster approximation are strongly dependent on the number surface and bulk atoms incorporated in the model, so quantitative predictions are not to be interpreted absolutely.

Simulations involving the aluminosilicate cluster were conducted using the basis set 6-31G* for the hydrocarbon fragment and the acidic hydrogen, 6-31 + G* for the bridging oxygen, and 3-21G* for silicon, aluminum, and the six terminating hydroxyl groups. Detailed information about the methods used can be found elsewhere (56, 57). The calculations were performed using the software package GAUSSIAN 94® (58) on IBM SP2 and DEC-alpha computers. Structural parameters were determined by optimizing to stationary points on the potential energy surface (PES) corresponding either to the stoichiometry $C_6H_{13}^{\oplus}$, $C_6H_{13}OH_2^{\oplus}$, or $C_6H_{13}OSiAl(OH)_6$ using the Berny algorithm and redundant internal coordinates (59). Carbenium and alkoxonium ions were optimized fully, whereas $C_6H_{13}OSiAl(OH)_6$ clusters were optimized partially by constraining the SiO_tH, AlO_tH, O_bSiO_tH, and O_bAlO_tH angles to values of 129.8°, 129.9°, 180.0°, and 180.0°, respectively, obtained from an optimization of the bare acid site, where O_t and O_b represent terminal and bridging oxygen atoms, respectively.

Transition states were located on the corresponding PES to estimate activation energies for the isomerization of hexyl cations in the gas phase and interacting with water and aluminosilicate sites. The location of transition states employed a STQN method, which uses a linear or quadratic synchronous transit approach to get closer than an initial guess to the quadratic region of the PES, followed by a quasi-Newton or eigenvalue-following algorithm to complete the optimization (60). Optimization criteria consisted of maximum and root-mean-squared forces of less than 22 and 15 J/mol-pm, respectively. The clusters resulting from optimizations were classified as local minima or transition states on the PES by calculating the Hessian matrix analytically. For local minima, the eigenvalues of the Hessian matrix were all positive, whereas for transition states only one eigenvalue was negative (54). Vibrational frequencies obtained from analyses of force constants were used further without scaling to estimate thermochemical properties of the clusters at 298 K. Typically, the error associated with the use of DFT methods for the estimation of reaction energetics is less or equal to 20 kJ/mol (56, 57), depending on the energy functional, basis sets, and size of the molecular cluster used. To verify that the transition states correspond to the chemical reactions of interest, intrinsic reaction coordinate calculations were performed using

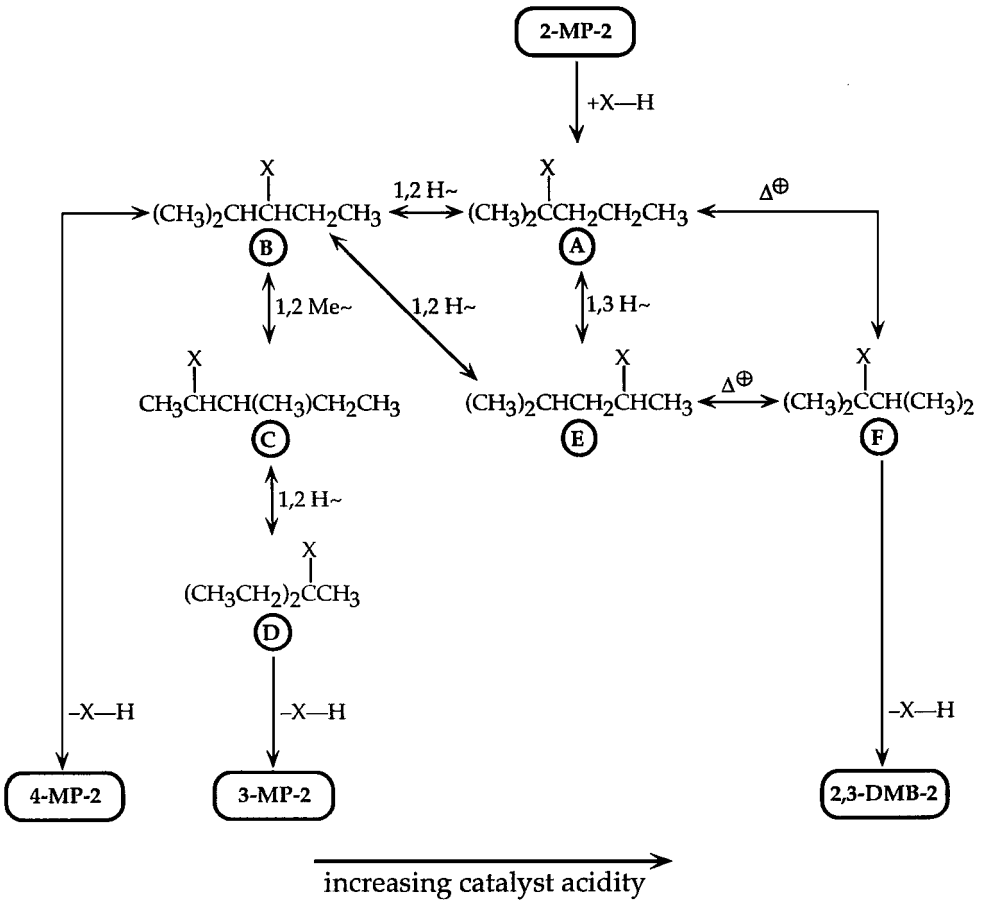

FIG. 1. Reaction scheme for isomerization of 2-methyl-pentene-2 (2-MP-2) to 4-methyl-pentene-2 (4-MP-2), 3-methyl-pentene-2 (3-MP-2), and 2,3-dimethyl-butene-2 (2,3-DMB-2) over the acid H–X. The symbol X is replaced by a positive charge for transformations of gaseous carbenium ions.

mass-weighted internal coordinates to follow the reaction paths in forward and reverse directions from the first-order saddle points (61–63).

3. RESULTS

3.1. Intermediates in the Isomerization Scheme

The conversion of 2-MP-2 to produce 4-MP-2, 3-MP-2, and 2,3-DMB-2 can be described as proceeding through protonation of 2-MP-2 to form the tertiary species 2-methyl-pentyl-2 (A), as shown in Fig. 1, which can subsequently react through one of three pathways. First, species A can undergo rearrangement to the secondary species 2-methyl-pentyl-3 (B) through a 1,2-hydride migration, followed by deprotonation to yield the alkene 4-MP-2. Alternatively, species B can undergo consecutive methyl and hydride migrations to form the tertiary species 3-methyl-pentyl-3 (D), whose subsequent deprotonation yields 3-MP-2. Finally, species A can undergo two types of branching rearrangements to produce 2,3-DMB-2. One pathway consists of a direct branching rearrangement of species A to the tertiary species 2,3-dimethyl-butyl (F), whose subsequent deprotonation yields 2,3-DMB-2. The second pathway involves the formation of the secondary species 4-methyl-pentyl-2 (E) via 1,3-hydride shift, followed by the branching rearrangement of this species to species F. This second pathway can also lead to the formation of species B and, thus, to the production of 4-MP-2 and eventually to the formation of 3-MP-2 through a subsequent 1,2-hydride shift.

Optimized structures of the hexyl cations involved in the gaseous conversion of 2-MP-2 are shown in Fig. 2. Structural parameters and relative energies are listed in Tables 1 and 2, respectively. In general, energies for gaseous secondary cations are calculated to be 40–50 kJ/mol higher than those for tertiary cations, in agreement with literature data (13, 14, 64). All hexyl cations in our study exhibit sp^2-hybridization of the carbon atom bearing the formal charge, indicating the presence of an empty p-orbital. All carbenium ions exhibit distortions such as elongation of C–H (or C–C) bonds and reduction of CCH (or CCC) angles resulting from hyperconjugative interactions (50). These interactions minimize the energy of the cations by maximizing the overlap between the vacant p-orbital at the formal cationic center and nearby, occupied orbitals from the aforementioned bonds. To highlight these effects in Fig. 2, elongated C–H bonds (∼112 pm) are marked by black hydrogen atoms, whereas typical C–H bond lengths of 109–110 pm are identified by shadowed hydrogen atoms. These elongated bonds are oriented nearly parallel to the vacant p-orbital. Moreover, secondary cations B, C, and E exhibit additional interactions between their cationic centers and adjacent C–C bonds, leading to low values for specific CCC angles (that is, values from 80° to 90°). The incorporation of diffuse

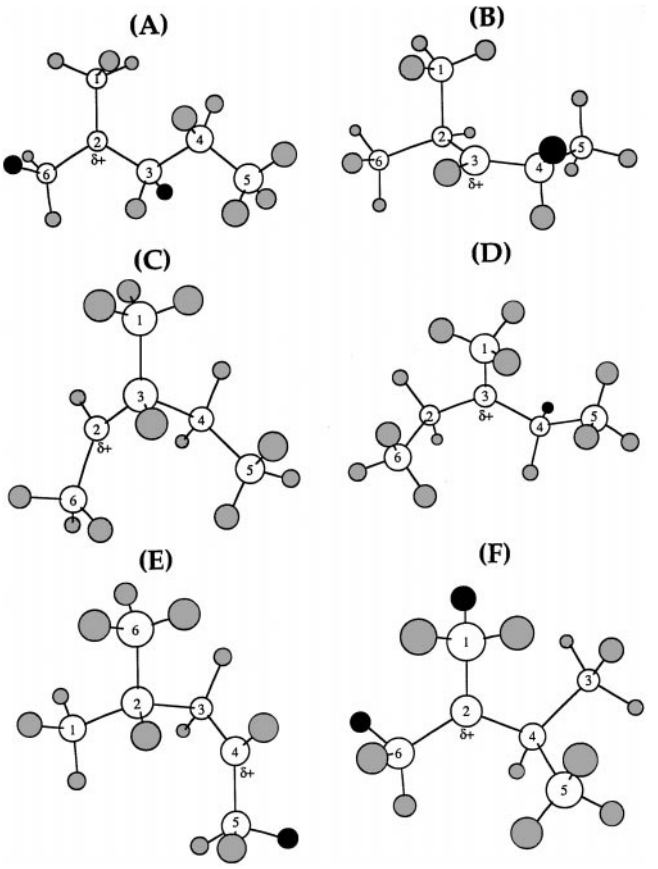

FIG. 2. Structures of (A) 2-methyl-pentyl-2, (B) 2-methyl-pentyl-3, (C) 3-methyl-pentyl-2, (D) 3-methyl-pentyl-3, (E) 4-methyl-pentyl-2, and (F) 2,3-dimethyl-butyl-2 cations. "Shadowed" hydrogen atoms form C–H bonds of a typical length within 109 to 110 pm, whereas "black" hydrogen atoms form elongated C–H bonds of lengths greater than 111 pm, due to hyperconjugative interactions. Structural parameters for the optimized cations in this figure are listed in Table 1.

functions into the basis set 6-31G* does not affect significantly the relative energies of the reactive intermediates; however, these additional functions accentuate the effects of hyperconjugative interactions involving C–C bonds on the structure of the secondary cations B, C, and E.

In the presence of a water molecule, the carbon atom bearing the positive charge in gaseous hexyl cations rehybridizes to a state between sp^2 and sp^3 when it interacts with the oxygen atom to form an alkoxonium ion. Optimized structures of the alkoxonium ions formed from cations A, B, C, D, and F are shown in Fig. 3, and their structural parameters and relative energies are listed in Tables 3 and 4, respectively. The (attractive) energies of interaction, $-\Delta E_w$, between water and the gaseous carbenium ions are also listed in Table 4. The energetic difference of ∼45 kJ/mol between secondary and tertiary cations in the gas phase is lower by ∼20 kJ/mol for the corresponding alkoxonium ions, since gaseous secondary cations B and C are stabilized more by interactions with water than are the tertiary cations

TABLE 1

Structural Parameters Obtained Using the Basis Set 6-31G* for the Optimized Reactants and Products Shown in Fig. 2

	A	B	C	D	E	F
Distances (pm)						
C_1C_2	147 (147)	164 (153)	—	—	153 (153)	147 (147)
C_2C_3	147 (147)	143 (143)	141 (141)	147 (147)	169 (168)	—
C_3C_4	153 (153)	146 (146)	171 (152)	147 (147)	141 (141)	153 (153)
C_4C_5	153 (153)	153 (153)	152 (153)	153 (153)	147 (147)	160 (160)
C_1C_3	—	—	152 (171)	147 (147)	—	
C_2C_4	—	—	—	—	—	146 (146)
C_2C_6	147 (147)	153 (164)	148 (148)	158 (158)	153 (153)	147 (147)
HC_2	—	109	109	109–110	110	—
HC_3	110, 112	109	109	—	109	109–110
HC_4	110	110, 112	109–110	110, 111	109	110
Angles (°)						
$C_1C_2C_3$	121.0 (121.2)	90.7 (118.6)	—	—	106.7 (107.7)	—
$C_2C_3C_4$	120.4 (120.4)	128.0 (128.0)	81.3 (122.0)	119.3 (119.3)	88.4 (88.8)	—
$C_3C_4C_5$	111.5 (111.5)	119.8 (119.9)	109.8 (114.2)	119.7 (119.8)	125.6 (125.7)	110.9 (111.0)
$C_1C_2C_6$	119.3 (119.3)	110.4 (110.4)	—	—	116.0 (116.0)	118.8(118.8)
$C_1C_3C_4$	—	—	112.4 (113.9)	120.8 (120.9)	—	
$C_2C_3C_1$	—	—	121.8 (77.8)	119.9 (119.9)	—	—
$C_2C_4C_3$	—	—	—	—	—	117.9 (117.7)
$C_2C_4C_5$	—	—	—	—	—	101.3 (101.8)
$C_6C_2C_3$	119.5 (119.5)	118.8 (91.3)	125.9 (126.0)	106.5 (106.6)	107.7 (107.0)	—
$C_6C_2C_4$	—	—	—	—	—	119.9 (120.0)
$C_1C_2C_4$	—	—	—	—	—	121.2 (121.2)

Note. Values in parenthesis correspond to the use of the basis set 6-31 + G*.

A, D, and F. Specifically, the stabilization energy changes associated with the interaction of water with secondary and tertiary hexyl cations to form alkoxonium ions are 72 and 40–53 kJ/mol (Table 4), respectively. Therefore, the energies of alkoxonium ions are less sensitive to their primary, secondary, or tertiary nature when compared to gaseous carbenium ions. The distance between the cationic center in the hydrocarbon and the oxygen atom in water is predicted to range from 164 to 174 pm. This distance is comparable to the typical length of 143 pm for C–O bonds, suggesting that these two atoms interact covalently. According to Mulliken population analyses (Fig. 3), about 60% of the total positive

TABLE 2

Energetics (kJ/mol) Predicted Using the Basis Set 6-31G* for Various Pathways Involved in the Isomerization of Isolated Hexyl Cations

	ΔE^a		ΔH		ΔG	
Overall reactions						
2-MP-2 + $H^{\oplus}$ → A	−866	(−866)	−841	(−841)	−846	(−846)
A → B	45	(45)	48	(49)	52	(52)
B → C	−5	(4)	−3	(5)	−2	(4)
C → D	−44	(−53)	−47	(−54)	−50	(−54)
A → E	47	(47)	51	(51)	56	(56)
A → F	−5	(−4)	−2	(−2)	1	(1)
Transition states						
A → TS1	72	(72)	70	(70)	75	(75)
A → TS2	49	(49)	52	(52)	58	(58)
C → TS3	27	(18)	19	(11)	20	(14)
E → TS4	15	(15)	10	(10)	17	(17)
E → TS5	21	(21)	12	(12)	15	(15)
E → TS6	45	(45)	42	(42)	48	(48)
A → TS7	94	(94)	94	(94)	105	(104)

Note. Values in parenthesis correspond to the use of the basis set 6-31 + G*.

[a] These values have not been corrected by the corresponding changes in zero-point energies.

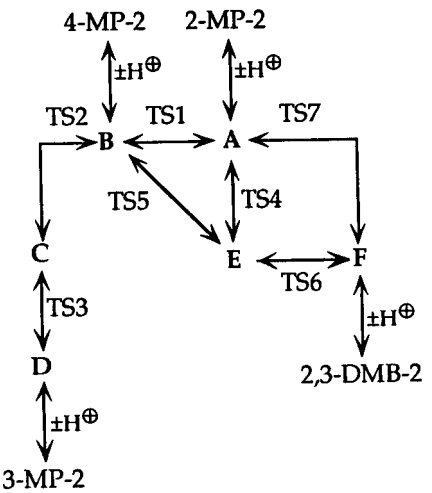

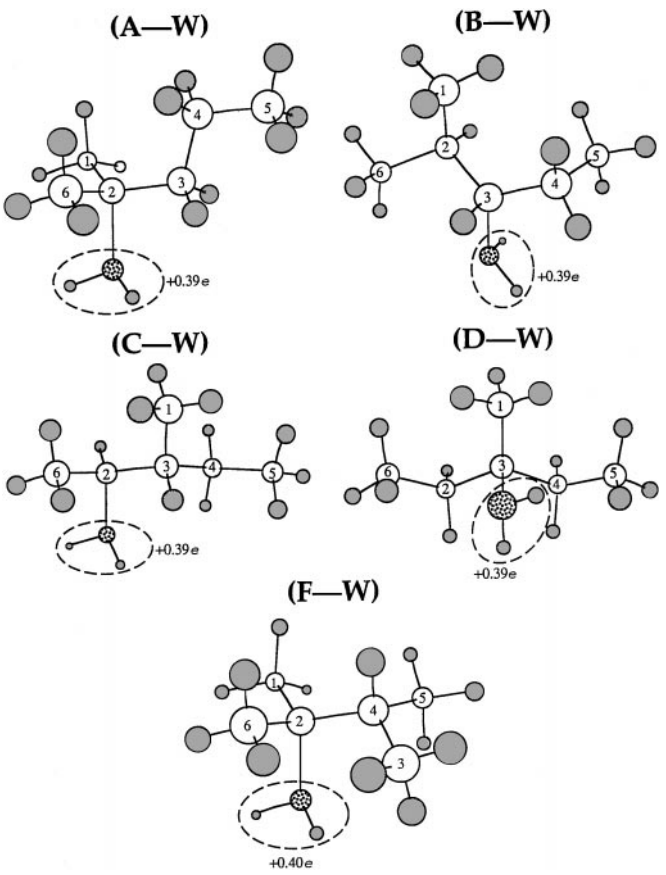

FIG. 3. Alkoxonium ions formed upon interaction of hexyl cations A, B, C, D, and F with water. Structural parameters for these optimized cations are listed in Table 3. The Mulliken charges included in this figure are associated with the H_2O fragment within each cluster.

charge is localized in the hydrocarbon fragment within the alkoxonium ions.

The interactions of alkenes with Brønsted acid sites on the surface of oxides such as aluminosilicates can lead to formation of π-complexes prior to their protonation and eventual formation of alkoxy species. Optimized structures of the π-complex and transition state involved in the protonation of 2-MP-2 are shown in Fig. 4. The π-complex formed upon adsorption of 2,3-DMB-2 is also shown in Fig. 4. Structural parameters are listed in Tables 5 and 6, while relative energies are listed in Table 7. As reported elsewhere for adsorption of isobutene on silica (27), the formation of π-complexes results mainly in perturbation of the C=C bond by surface hydroxyl groups. The energy of formation associated with π-complexes is predicted to be -62 ± 4 kJ/mol (Table 7), and it is relatively independent of the nature of the adsorbed hexene. The Mulliken charge of the hydrocarbon fragment of the transition state is $+0.48e$ versus the value of $-0.08e$ for the π-complex, and the activation energy for protonation, thus, depends on the ability of the surface to donate a proton to the adsorbed alkene. The activation energy for the protonation of 2-MP-2 to form a tertiary alkoxy species is predicted to be 71 kJ/mol relative to the π-adsorbed alkene. These results are in agreement with previous *ab initio* studies performed by Kazansky and coworkers (19, 32, 34) for the protonation of ethene over H-zeolites, which led to an activation energy of 64 kJ/mol relative to π-adsorbed ethene.

It has been suggested (65–68) that the acid strength of a site can be represented theoretically by the deprotonation energy of a representative cluster (and this value is equal to the proton affinity of the conjugate basic form of the site). The deprotonation energy is defined as the energy required to remove a proton from the cluster, and it decreases as the acid strength of the cluster increases. The deprotonation energy of the aluminosilicate cluster used throughout our studies is 1420 kJ/mol (Table 7), and this value is within the range of 1000 to 1600 kJ/mol found by Sauer, Kazansky,

TABLE 3

Structural Parameters for the Optimized Alkoxonium Ions Shown in Fig. 3

	A–W	B–W	C–W	D–W	F–W
Distances (pm)					
C_1C_2	151	155	—	—	151
C_2C_3	152	152	152	152	—
C_3C_4	155	152	155	152	154
C_4C_5	153	153	153	154	154
C_1C_3	—	—	155	151	—
C_2C_4	—	—	—	—	154
C_2C_6	151	154	151	153	152
HC_2	—	110	109	110	—
HC_3	110	109	110	—	109, 110
HC_4	110	110	110	110	110
HO	98	98	98	98	98
C_2O	174	—	164	—	170
C_3O	—	164	—	171	—
Angles (°)					
$C_1C_2C_3$	116.4	108.0	—	—	—
$C_2C_3C_4$	112.8	120.7	112.4	113.7	—
$C_3C_4C_5$	111.0	116.8	113.8	118.0	110.5
$C_1C_2C_6$	115.7	110.5	—	—	113.5
$C_1C_3C_4$	—	—	111.9	116.7	—
$C_2C_3C_1$	—	—	107.7	116.4	—
$C_2C_4C_3$	—	—	—	—	114.3
$C_2C_4C_5$	—	—	—	—	114.5
$C_6C_2C_3$	116.6	112.5	119.4	117.8	—
$C_6C_2C_4$	—	—	—	—	116.3
$C_1C_2C_4$	—	—	—	—	116.5
C_1C_2O	100.0	—	—	—	100.7
C_3C_2O	100.0	—	104.8	—	—
C_4C_2O	—	—	—	—	102.4
C_6C_2O	104.0	—	106.2	—	104.4
HC_2O	—	—	97.8	—	—
C_1C_3O	—	—	—	100.7	—
C_2C_3O	—	104.5	—	101.2	—
C_4C_3O	—	106.7	—	105.0	—
HC_3O	—	97.7	—	—	—
HOH	107.8	108.0	108.3	107.6	108.0

TABLE 4

Energetics (kJ/mol) Predicted for Various Pathways Involved in the Isomerization of Alkoxonium Ions Formed upon Interaction of the Hexyl Cations Shown in Fig. 2 with Water

	ΔE^a	ΔH	ΔG	Experimental[b]
Overall reactions				
$H_3O^{\oplus} \rightarrow H_2O + H^{\oplus}$	706	671	675	
2-MP-2 + $H_3O^{\oplus} \rightarrow$ A–W	−199	−191	−142	
A–W → B–W	26	29	31	
B–W → C–W	4	3	2	
C–W → D–W	−25	−27	−26	
A–W → F–W	9	8	11	
Transition states				
A–W → TS1–W	58	43	30	~46
A–W → TS2–W	66	58	46	58
C–W → TS3–W	34	18	5	~8
A–W → TS7–W	104	92	83	73
Heats of formation ($-\Delta E_w$): I–W → I + W				
A–W	53			
B–W	72			
C–W	72			
D–W	44			
F–W	40			
TS1–W	66			
TS2–W	35			
TS3–W	56			
TS7–W	42			

[a] These values have not been corrected by the corresponding changes in zero-point energies.

[b] These values correspond to transformations in liquid, superacidic media as reported in Refs. (13) and (14).

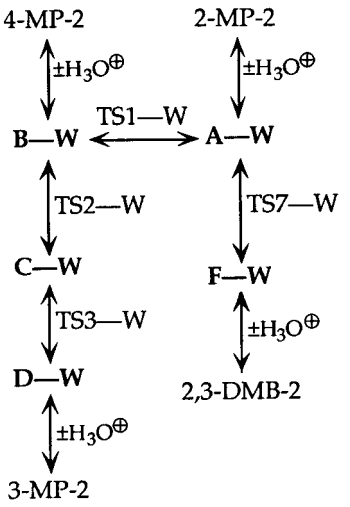

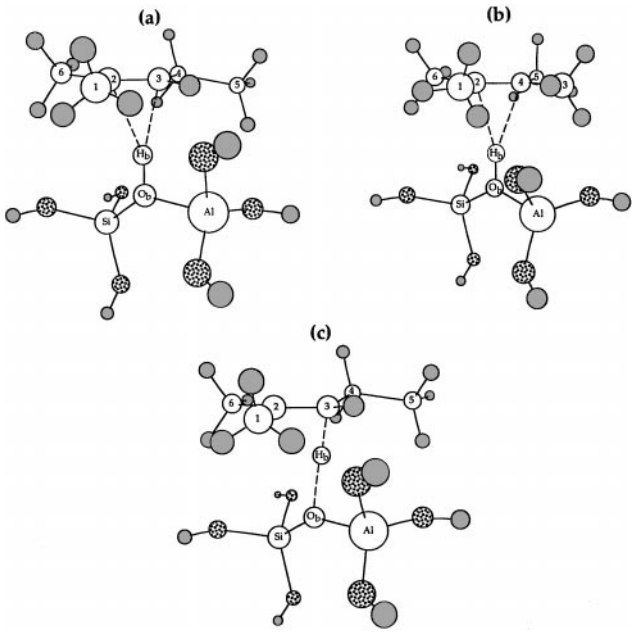

FIG. 4. π-complexes formed upon adsorption of (a) 2-MP-2 and (b) 2,3-DMB-2 on an aluminosilicate site. The transition state for the protonation of Fig. a is shown in Fig. c. The structural parameters are listed in Tables 5 and 6.

and their coworkers (65, 67, 68) for various models of Brønsted acid sites on aluminosilicates. In comparison, the deprotonation energy of the hydronium ion (equal to the proton affinity of water) is calculated to be 706 kJ/mol (Table 4), reflecting the fact that the hydronium ion is a stronger acid than the neutral aluminosilicate cluster.

The protonation and further reaction of 2-MP-2 over aluminosilicates yields a series of alkoxy species, and their optimized structures are shown in Fig. 5. Structural parameters and relative energies are listed in Tables 5 and 7. The values of CCC and CCH angles in Table 5 indicate that the carbon atom nearest to the bridging oxygen is sp^3-hybridized, in contrast to the sp^2 hybridization within the gaseous carbenium ions. In addition, the C–O distances of 150–155 pm are only slightly longer than the value of 143 pm which is typical of single C–O bonds, thus suggesting that these two atoms interact covalently. Therefore, these hexyl species are alkoxy species associated with the aluminosilicate cluster. Importantly, the energies of formation of the various alkoxy species (-74 ± 14 kJ/mol on average) are relatively independent of their primary, secondary, or tertiary nature. Mulliken charges associated with the hydrocarbon fragments of the alkoxy species in Fig. 5 range from $+0.25e$ to $+0.30e$.

TABLE 5

Structural Parameters for the Optimized π-Complexes and Hexyl (Alkoxy) Species on an Aluminosilicate Site as Shown in Figs. 4 and 5

	2-MP-2 (π)	2,3-DMB-2 (π)	A-X	B-X	C-X	D-X	F-X
distances (pm)							
C_1C_2	151	152	153	154	—	—	153
C_2C_3	135	—	154	154	154	154	—
C_3C_4	152	151	154	153	155	154	154
C_4C_5	154	152	153	153	153	154	154
C_1C_3	—	—	—	—	154	153	—
C_2C_4	—	136	—	—	—	—	156
C_2C_6	151	152	153	154	152	154	153
H_bC_2	212	210	—	—	—	—	—
H_bC_3	199	—	—	—	—	—	—
H_bC_4	—	211	—	—	—	—	—
H_bO_b	100	101	—	—	—	—	—
O_bC_2	307	307	155	—	151	—	155
O_bC_3	297	—	—	152	—	155	—
O_bC_4	—	308	—	—	—	—	—
O_bSi	166	166	167	167	167	169	168
O_bAl	191	191	195	192	192	192	197
O_tSi	162-164	162-164	162-164	162-164	162-164	163-165	162-164
O_tAl	171-174	171-173	172-174	172-174	172-173	172-173	172-174
angles (°)							
$C_1C_2C_3$	120.9	—	114.8	110.4	—	—	—
$C_2C_3C_4$	127.4	—	115.2	119.8	111.0	113.0	—
$C_3C_4C_5$	111.9	113.4	111.5	112.3	114.2	114.7	109.2
$C_1C_2C_6$	115.6	114.0	110.7	111.0	—	—	107.4
$C_1C_3C_4$	—	—	—	—	112.5	110.0	—
$C_2C_3C_1$	—	—	—	—	108.6	113.4	—
$C_2C_4C_3$	—	123.3	—	—	—	—	114.7
$C_2C_4C_5$	—	123.3	—	—	—	—	114.2
$C_6C_2C_3$	123.5	—	112.2	117.7	116.7	115.3	—
$C_6C_2C_4$	—	123.3	—	—	—	—	112.0
$C_1C_2C_4$	—	122.7	—	—	—	—	113.8
$H_bC_2C_3$	65.6	—	—	—	—	—	—
$H_bC_3C_2$	76.2	—	—	—	—	—	—
$H_bC_2C_4$	—	71.7	—	—	—	—	—
$H_bC_4C_2$	—	70.7	—	—	—	—	—
H_tO_tSi	129.8	129.8	129.8	129.8	129.8	129.8	129.8
H_tO_tAl	129.9	129.9	129.9	129.9	129.9	129.9	129.9
O_tSiO_b	104.3-105.4	104.2-105.4	105.2-106.0	104.9-107.0	102.4-107.0	104.2-109.0	105.3-107.4
O_tAlO_b	93.0-105.4	96.5-103.9	101.2-102.0	98.9-101.4	96.4-102.0	91.9-104.6	92.7-110.7
AlO_bSi	137.8	140.4	116.4	119.7	118.8	114.4	112.6

3.2. Transition States in the Isomerization Scheme

3.2.1. Production of 4-MP-2 (TS1)

The optimized structure of the transition state (TS1) for the 1,2-hydride migration involved in the isomerization of A to B is shown in Fig. 6. Energetic and structural parameters of TS1 are listed in Tables 2 and 8. The activation energies for the forward and reverse reactions are predicted to be 72 kJ/mol and 27 kJ/mol, respectively. Uncertainties in these energies can be caused by inaccurate accounting of electron-correlation effects by the DFT method, since the proper inclusion of electron-correlation energies is crucial when modelling the behavior of carbenium ions (50–52). Nevertheless, the results of our calculations are in agreement with previous DFT and *ab initio* studies (52) of secondary to tertiary 1,2-hydride shifts in methyl–butyl cations, which have predicted the activation energy to be between 12 and 32 kJ/mol.

The C–H bond involving the migrating hydrogen atom in TS1 is nearly parallel to the empty p-orbital in atom C_3, which bears the formal charge. This prediction is in agreement with the suggestion of Brouwer (13, 14) that the vacant p-orbital in the formal cationic center becomes coplanar with the sp^3-orbital carrying the migrating entity for a 1,2-shift to achieve maximum stability of the transition state. Mulliken population analyses indicate that TS1 resembles a secondary cation whose positive charge is localized mainly in atom C_3.

The presence of a water molecule has a significant effect on the energetics for the 1,2-hydride migration involved in the isomerization of A to B. The optimized structure for this transition state (TS1–W) is shown in Fig. 7, and the

TABLE 6

Structural Parameters for Transition States of 2-MP-2 Protonation and Isomerization Reactions on an Aluminosilicate Site as Shown in Figs. 4 and 8

	2-MP-2 protonation	TS1-X	TS2-X	TS3-X	TS7-X
distances (pm)					
C_1C_2	150	151	189	—	153
C_2C_3	140	141	140	141	152
C_3C_4	152	150	151	151	179
C_4C_5	154	153	153	153	151
C_1C_3	—	—	179	150	—
C_2C_4	—	—	—	—	151
C_2C_6	149	150	149	148	153
HC_2	174	133	—	134	—
HC_3	125	132	—	132	126
HC_4	—	—	—	—	133
O_bC_2	296	321	324	287	334
O_bC_3	281	281	297	332	274
O_bSi	160	157	157	158	157
O_bAl	180	177	176	176	177
O_tSi	163-166	164-167	164-167	164-168	164-167
O_tAl	172-176	172-179	172-179	172-177	173-180
angles (°)					
$C_1C_2C_3$	118.0	118.6	63.9	—	115.5
$C_2C_3C_4$	126.7	126.5	123.5	121.8	53.4
$C_3C_4C_5$	110.6	112.8	113.0	116.2	116.2
$C_1C_2C_6$	118.5	117.3	109.3	—	113.3
$C_1C_3C_4$	—	—	—	117.6	—
$C_2C_3C_1$	—	—	71.6	118.7	—
$C_2C_4C_3$	—	—	—	—	54.0
$C_2C_4C_5$	—	—	—	—	121.2
$C_6C_2C_3$	122.8	122.9	123.0	126.7	115.3
$C_6C_2C_4$	—	—	—	—	114.9
$H^*C_2C_3$	45.3	57.6	—	57.2	—
$H^*C_2C_4$	—	—	—	—	—
$H^*C_3C_2$	81.9	58.4	—	58,8	100.7
$H^*C_3C_4$	—	—	—	—	47.9
$H^*C_4C_3$	—	—	—	—	45.0
$O_bC_2C_3$	70.0	61.0	66.5	95.6	53.9
$O_bC_2C_4$	—	—	—	—	123.0
$O_bC_3C_4$	82.0	92.9	88.0	59.4	99.4
H_tO_tSi	129.8	129.8	129.8	129.8	129.8
H_tO_tAl	129.9	129.9	129.9	129.9	129.9
O_tSiO_b	105.8-111.3	107.5-112.0	107.0-112.0	105.0-111.0	106.7-112.4
O_tAlO_b	98.7-108.8	100.3-111.0	100.6-110.9	102.8-111.2	100.0-110.0
AlO_bSi	147.0	158.8	166.3	158.7	158.8

energetic and structural parameters are listed in Tables 4 and 9, respectively. The activation energies for the forward and reverse reactions are predicted to be 58 and 32 kJ/mol, respectively. These predictions are higher than the values of 46 and 8 kJ/mol reported by Brouwer and coworkers (13, 14) for 1,2-hydride migrations from tertiary to secondary carbenium ions in superacidic solutions. Calculated enthalpies of activation are in better agreement with these experimental barriers. Nevertheless, our predictions are within the error expected from DFT calculations (56, 57). It should be noted that since TS1 and B are secondary cations, they are stabilized by interactions with water more than the tertiary cation A; stabilization energies are estimated to be 53, 72, and 66 kJ/mol for interactions of A, B, and TS1, respectively, with water (Table 4). Therefore, the activation energy for the tertiary to secondary 1,2-hydride migration in the presence of water is lower than in the gas phase, while the activation energy for the secondary to tertiary reaction is slightly higher.

The Mulliken charge associated with the hydrocarbon fragment in TS1–W is increased to 98% of the total charge, as shown in Fig. 7, and this charge is mainly localized on atom C_3. Therefore, the isomerization process involves a separation of electronic charge within the transition state.

TABLE 7

Energetics (kJ/mol) Predicted for Various Pathways Involved in the Isomerization of Hexyl Species over an Aluminosilicate Site

	ΔE^a	ΔH	Experimental[b]
Overall reactions			
H-X → $H^{\oplus} + X^{-}$	1420		
2-MP-2 → 4-MP-2 (*trans*)	6	5	5
2-MP-2 → 3-MP-2 (*trans*)	3	3	4
2-MP-2 → 2,3-DMB-2	1	0	−1
Intermediates			
2-MP-2—H-X (π)	−65		
A-X	−73		
B-X	−77		
C-X	−93		
D-X	−70		
F-X	−56		
2,3-DMB-2—H-X (π)	−58		
Transition states			
TS(2-MP-2 protonation)-X	6		
TS1-X	41		22–52
TS2-X	71		55–68
TS3-X	52		
TS7-X	117		

Note. Energies of the reactive intermediates and transition states are reported relative to 2-MP-2 + H-X, where X represents the conjugate base of the acid site.

[a] These values have not been corrected by the corresponding changes in zero-point energies.

[b] Overall heats of reaction are calculated from data in standard thermodynamic tables. Apparent activation energies correspond to reactions over amorphous silica-alumina and ultrastable Y-zeolite as reported in Ref. (45).

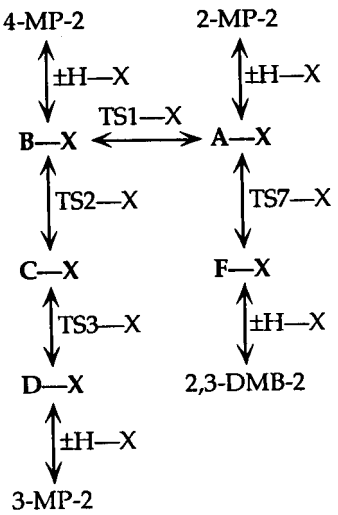

This view is also supported by the long C_2–O and C_3–O distances of 324 and 273 pm, respectively, which suggest that TS1–W consists essentially of a carbenium ion (TS1) and neutral water.

The optimized structure of TS1 interacting with the aluminosilicate cluster (H-X) is shown in Fig. 8. Structural parameters and reactions energetics are listed in Tables 6 and 7, respectively. The activation energy for the forward reaction (A-X → B-X) is predicted to be 41 kJ/mol relative to gaseous 2-MP-2 plus the acid site. As in the analogous case involving alkoxonium ions, the activation of A-X to produce B-X via 1,2-hydride shift requires the separation of charge, leading to a transition state that resembles a carbenium ion plus the conjugate basic form of the oxide cluster: Mulliken charges for the hydrocarbon fragments within A-X and B-X are +0.30*e* and +0.26*e*, whereas this charge is increased to +0.51*e* within TS1-X. The existence of a carbenium ion within TS1-X is also evident from the long C_2–O and C_3–O distances and the predicted rehybridization of these carbon atoms from a sp^3 state in the alkoxy species to a nearly sp^2 state in the transition state.

3.2.2. Production of 3-MP-2: 1,2-Methyl Shift (TS2)

The optimized structure of the transition state (TS2) for the 1,2-methyl migration involved in the isomerization of B to C is shown in Fig. 6, and the energetic and structural parameters are listed in Tables 2 and 8. The activation energies for the forward and reverse reactions are both predicted to be lower than 10 kJ/mol. The main feature observed in the structure of TS2 is a three-center, two-electron bond involving atoms C_2, C_3, and the migrating atom C_1. The C_1–C_2 and C_1–C_3 distances are near 187 and 180 pm while the $C_1C_2C_3$ and $C_2C_3C_1$ angles are approximately 65° and 70°, respectively. This symmetric position of the migrating methyl group is expected on the basis of the small energetic difference between the stable species involved in the reaction. The Mulliken charges associated with atoms C_1 through C_6 in TS2 indicate that the positive charge is not localized in a specific carbon atom, but that it is delocalized in the $C_1C_2C_3$-ring.

The presence of a water molecule has a significant effect on the isomerization of species B to C. The optimized

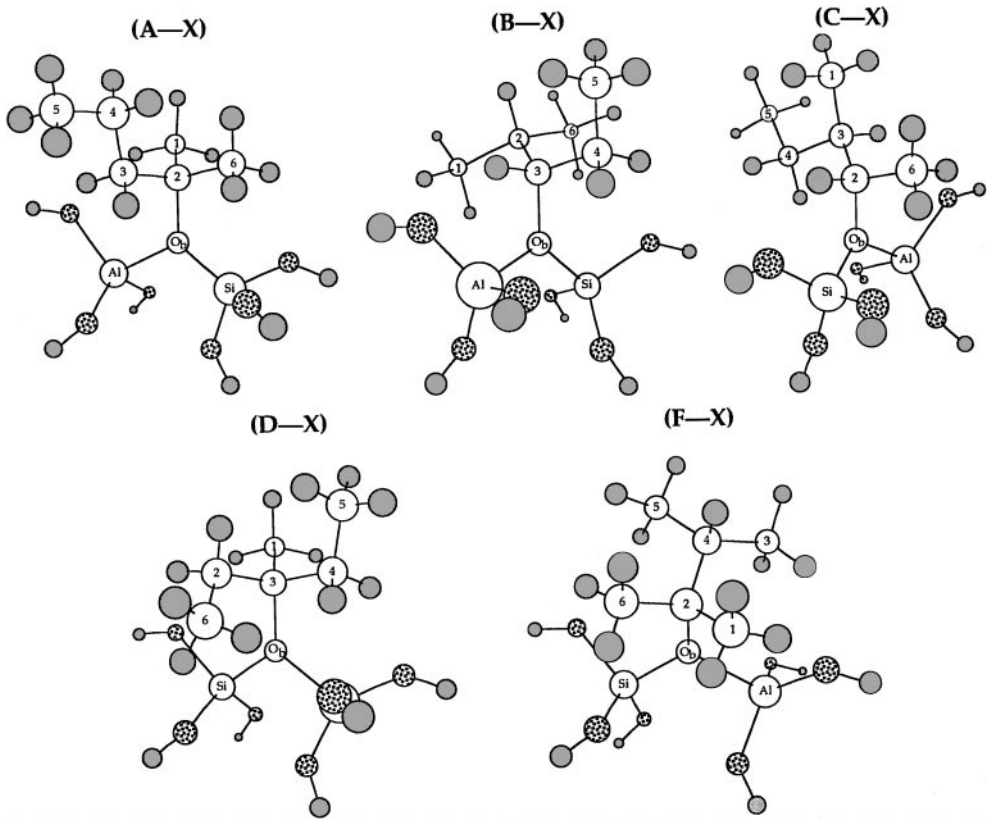

FIG. 5. Hexyl (alkoxy) species formed upon adsorption and reaction of 2-MP-2 and its isomers on an aluminosilicate site. The structural parameters are listed in Table 5.

structure of TS2 interacting with water is shown in Fig. 7, and the corresponding energetic and structural parameters are listed in Tables 4 and 9, respectively. The activation energies for the forward and reverse reactions are predicted to be 40 and 36 kJ/mol, respectively, and these values are higher than the experimental value of 14 kJ/mol reported by Brouwer and coworkers (13, 14). The stabilization energies associated with the formation of alkoxonium ions from interactions of B and C with water are both near 72 kJ/mol (Table 4), whereas this value is 35 kJ/mol for TS2. Therefore, reactive intermediates are stabilized more than the transition state upon interaction with water, resulting in an increased activation energy. Mulliken charges (Figs. 3 and 7) indicate that nearly all the positive charge is localized in the hydrocarbon fragment within TS2–W. Moreover, the long C_2–O and C_3–O distances (305 and 322 pm, respectively) also suggest that TS2–W comprises essentially a free carbenium ion (TS2) and neutral water.

The optimized structure TS2 interacting with the aluminosilicate cluster is shown is Fig. 8. Structural parameters and reaction energetics are listed in Tables 6 and 7, respectively. The activation energy for the forward reaction (B-X $\rightarrow$ C-X) is predicted to be 71 kJ/mol relative to gaseous 2-MP-2 plus the acid site. As in the analogous case involving alkoxonium ions, the activation of B-X to produce C-X via 1,2-methyl shift requires the separation of charge, leading to a transition state that resembles a carbenium ion plus the conjugate basic form of the oxide cluster: Mulliken charges for the hydrocarbon fragments within B-X and C-X are $+0.26e$ and $+0.27e$, whereas this charge is increased to $+0.54e$ within TS2-X. The existence of a carbenium ion within TS2-X is also evident from the long C_2–O and C_3–O distances and the predicted rehybridization of these carbon atoms from a sp^3 state in the alkoxy species to a nearly sp^2 state in the transition state.

3.2.3. Production of 3-MP-2: 1,2-Hydride Shift (TS3)

The optimized structure of the transition state (TS3) for the 1,2-hydride migration involved in the isomerization of C to D is shown in Fig. 6, and energetic and structural parameters are listed in Tables 2 and 8. The activation energies for the forward and reverse reactions are predicted to be 27 (18) and 71 (71) kJ/mol, respectively, using the basis set 6-31G* (6-31 + G*). TS3 is similar to TS1, since it resembles a secondary cation; Mulliken charges in TS3 suggest that the positive charge is localized mainly in C_2. The angle formed between the C–H bond containing the migrating

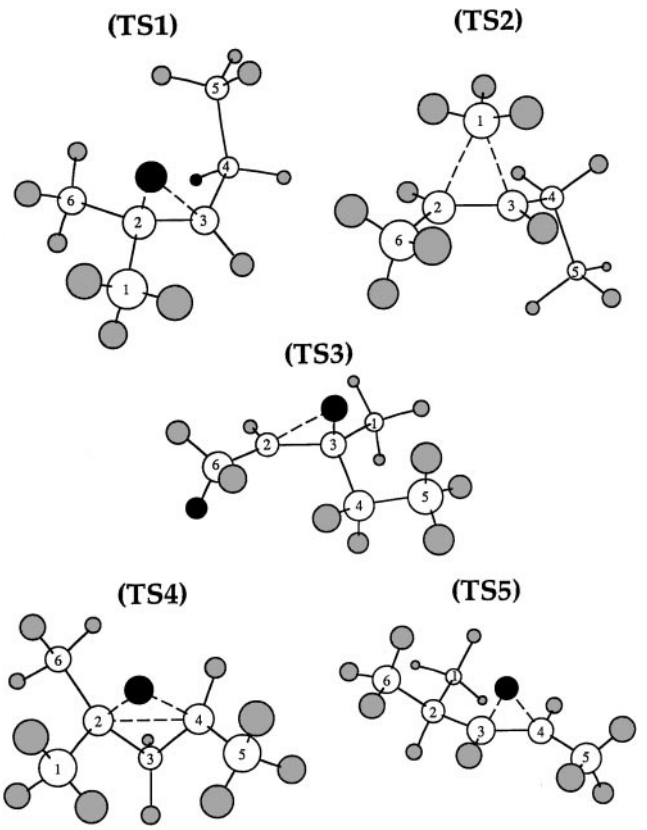

FIG. 6. Transition states of elementary reactions (TS1) A ↔ B, (TS2) B ↔ C, (TS3) C ↔ D, (TS4) A ↔ E, and (TS5) E ↔ B. The structural parameters are listed in Table 8.

hydrogen atom and the C_2–C_3 bond is 98°, showing that this C–H bond aligns with the vacant p-orbital in C_2.

The optimized structure of TS3 interacting with water is shown in Fig. 7, and the corresponding energetic and structural parameters are listed in Tables 4 and 9, respectively. The activation energies for the forward and reverse conversion of C to D are 34 and 59 kJ/mol upon interaction with water, and these values should be compared to the experimental values of 8 and 46 kJ/mol referred to previously. Calculated enthalpies of activation are in better agreement with these experimental barriers. Nevertheless, our predictions are within the error expected from DFT calculations (56, 57). The activation energy for the reverse reaction is lower by 12 kJ/mol than the gas-phase values, and this behavior is caused by the stronger interaction with water of secondary species C and TS3, compared to the tertiary species D. Stabilization energies for species C, TS3, and D are 72, 56, and 44 kJ/mol, respectively (Table 4). Furthermore, the isomerization process involves a separation of charge since 99% of the total is localized in the hydrocarbon fragment within TS3–W. The long C_2–O and C_3–O distances (268 and 324 pm, respectively) also suggest that TS3–W consists essentially of a carbenium ion (TS3) and neutral water.

The optimized structure of TS3 interacting with the aluminosilicate site is shown in Fig. 8. Structural parameters and reaction energetics are listed in Tables 6 and 7, respectively. The activation energy for the forward reaction (C-X → D-X) is predicted to be 52 kJ/mol relative to gaseous 2-MP-2 plus the bare acid site. As in the analogous case involving alkoxonium ions, the activation of C-X to produce D-X via 1,2-hydride shift requires the separation of charge, leading to a transition state that resembles a carbenium ion plus the conjugate basic form of the oxide cluster; Mulliken charges for the hydrocarbon fragment within C-X and D-X are both +0.26*e*, whereas this charge is increased to +0.51*e* within TS3-X. The existence of a carbenium ion within TS3-X is also evident from the long C_2–O and C_3–O distances and the predicted rehybridization of these carbon atoms from a sp^3 state in the alkoxy species to a nearly sp^2 state in the transition state.

3.2.4. Production of 2,3-DMB-2 (TS4, TS5, and TS6)

The production of 2,3-DMB-2 can take place through two pathways. The first pathway consists of consecutive 1,3-hydride migrations and branching rearrangements from species A, to species E, and then to species F. The second

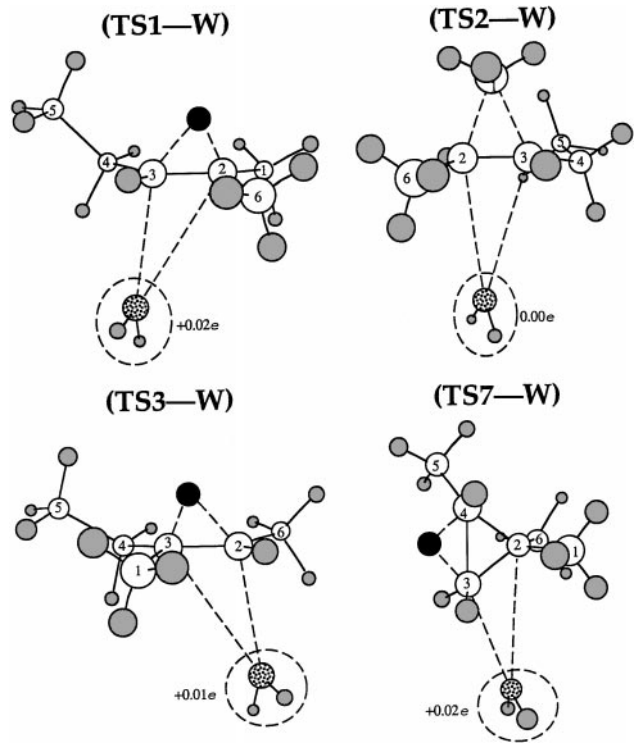

FIG. 7. Transition states of elementary reactions (TS1–W) A–W ↔ B–W, (TS2–W) B–W ↔ C–W, (TS3–W) C–W ↔ D–W, and (TS7–W) A–W ↔ F–W. The structural parameters are listed in Table 9. The Mulliken charges included in this figure are associated with the H_2O fragment within each cluster.

TABLE 8

Structural Parameters Obtained Using the Basis Set 6-31G* for Optimized Transition States Shown in Figs. 6 and 9

	TS1	TS2	TS3	TS4	TS5	TS6	TS7
distances (pm)							
C_1C_2	154 (154)	187 (186)	—	153 (153)	153 (153)	154 (154)	153 (153)
C_2C_3	145 (145)	140 (140)	145 (145)	154 (154)	152 (152)	183 (183)	147 (147)
C_3C_4	146 (146)	151 (151)	158 (158)	147 (148)	140 (140)	144 (144)	178 (178)
C_4C_5	155 (156)	154 (154)	153 (153)	150 (150)	148 (148)	152 (152)	152 (152)
C_1C_3	—	180 (180)	153 (153)	—	—	—	—
C_2C_4	—	—	—	189 (189)	—	161 (161)	157 (157)
C_2C_6	156 (156)	150 (150)	145 (145)	153 (153)	154 (154)	153 (154)	153 (153)
$H^{\bullet}C_2$	112 (112)	—	195 (195)	121 (122)	—	116 (116)	—
$H^{\bullet}C_3$	196 (197)	—	113 (113)	—	123 (123)	157 (157)	144 (145)
$H^{\bullet}C_4$	—	—	—	146 (146)	148 (147)	—	120 (120)
angles (°)							
$C_1C_2C_3$	114.5 (114.5)	65.0 (65.4)	—	115.6 (115.7)	114.4 (114.5)	119.9 (119.9)	116.8 (116.8)
$C_2C_3C_4$	127.9 (127.8)	125.2 (125.2)	114.5 (114.5)	77.4 (77.4)	126.4 (126.6)	57.5 (57.5)	56.8 (56.8)
$C_3C_4C_5$	118.2 (117.9)	109.6 (109.6)	112.9 (113.0)	123.4 (123.4)	125.6 (125.6)	121.5 (121.6)	124.8 (124.9)
$C_1C_2C_6$	112.9 (112.9)	114.2 (114.0)	—	117.6 (117.5)	112.6 (112.6)	117.6 (117.5)	113.9 (113.8)
$C_2C_3C_1$	—	70.0 (69.8)	114.8 (114.8)	—	—	—	—
$C_2C_4C_3$	—	—	—	52.9 (52.8)	—	73.4 (73.4)	51.5 (51.4)
$C_2C_4C_5$	—	—	—	122.0 (122.2)	—	119.3 (119.4)	120.4 (120.5)
$C_6C_2C_3$	115.6 (115.4)	124.9 (124.8)	127.4 (127.4)	114.9 (115.0)	110.0 (110.0)	122.0 (122.0)	117.7 (117.7)
$C_1C_3C_4$	—	110.0 (110.0)	114.8 (114.9)	—	—	—	—
$C_6C_2C_4$	—	—	—	118.7 (118.7)	—	114.2 (114.2)	116.4 (116.4)
$H^{\bullet}C_2C_3$	98.2 (98.6)	—	—	100.4 (100.4)	—	58.2 (58.4)	—
$H^{\bullet}C_2C_4$	—	—	—	50.7 (50.6)	—	107.3 (107.4)	—
$H^{\bullet}C_3C_2$	—	—	97.6 (97.7)	—	109.6 (109.9)	39.2 (39.0)	98.8 (98.8)
$H^{\bullet}C_3C_4$	—	—	—	—	68.0 (67.3)	96.7 (96.6)	42.0 (42.0)

Note. Values in parenthesis correspond to the use of the basis set 6-31 + G*.

pathway consists of a direct branching rearrangement from species A to species F.

The optimized structure of the transition state (TS4) for the 1,3-hydride migration involved in the isomerization of A to E is shown in Fig. 6, and energetic and structural parameters are listed in Tables 2 and 8. The activation energies for the forward and reverse reactions are predicted to be 62 and 15 kJ/mol, respectively, regardless of the basis set used. The activation energy for the reverse reaction, although within the expected error, is slightly lower than the value of 36 kJ/mol (13) for 1,3-hydride shifts within tertiary 2,4-dimethyl-pentyl cations. TS4 has a two-electron, three-center bond involving the migratory entity, but the overall structure of this edge-protonated cyclopropane ring is somewhat more complex than TS2. The HC_2C_4 angle of 51° and the relatively short C_2–C_4 distance of 189 pm suggest the formation of a partial bond between these two carbon atoms. In addition, Mulliken charges associated with the carbon atoms in TS4 suggest that the positive charge is delocalized within the HC_2C_4-ring.

Cation E can undergo a 1,2-hydride shift to form secondary cation B or a branching rearrangement to form tertiary cation F. The optimized structure of the transition state (TS5) for isomerization of species E to B is shown in Fig. 6, and energetic and structural parameters are listed in Tables 2 and 8. The activation energies for the forward and reverse reactions are both predicted to be near 22 kJ/mol, and they are ~10 kJ/mol higher than experimental values for 1,2-hydride shifts in secondary n-butyl cations (13, 14). The migrating hydrogen atom is positioned symmetrically between atoms C_3 and C_4, which are the atoms bearing the formal positive charge in cations B and E, respectively. A two-electron, three-center bond is formed involving the migratory entity, resulting in delocalization of the positive charge within the HC_3C_4-ring.

The branching rearrangement of species E to F proceeds via transition state TS6. The optimized structure for this transition state is shown in Fig. 9, and the energetic and structural parameters are listed in Tables 2 and 8, respectively. The activation energies for the forward and reverse reactions are predicted to be 45 and 97 kJ/mol, respectively. These results are in agreement with values of 71 to 85 kJ/mol obtained from previous DFT and *ab initio* calculations (52) of the activation energy for the secondary to tertiary branching rearrangement of *n*-pentyl to methylbutyl cations.

TS6 resembles a protonated cyclopropane ring. The forward reaction requires not only the migration of a hydrogen

TABLE 9

Structural Parameters for the Optimized Transition States Shown in Fig. 7

	TS1—W	TS2—W	TS3—W	TS7—W
distances (pm)				
C_1C_2	152	183	—	153
C_2C_3	141	139	142	148
C_3C_4	148	150	153	180
C_4C_5	154	153	154	152
C_1C_3	—	185	152	—
C_2C_4	—	—	—	155
C_2C_6	152	150	148	153
$H^{\bullet}C_2$	123	—	152	—
$H^{\bullet}C_3$	149	—	122	139
$H^{\bullet}C_4$	—	—	—	123
C_2O	324	305	268	337
C_3O	273	322	324	272
HO	97	97	97	97
angles (°)				
$C_1C_2C_3$	118.9	68.8	—	116.0
$C_2C_3C_4$	128.8	126.4	122.0	55.0
$C_3C_4C_5$	113.8	117.5	114.8	124.4
$C_1C_2C_6$	116.0	109.0	—	113.3
$C_2C_3C_1$	—	66.7	117.9	—
$C_2C_4C_3$	—	—	—	51.8
$C_2C_4C_5$	—	—	—	121.8
$C_6C_2C_3$	122.6	124.8	129.0	117.0
$C_1C_3C_4$	—	114.7	117.2	—
$C_6C_2C_4$	—	—	—	117.2
$H^{\bullet}C_2C_3$	68.0	—	48.9	—
$H^{\bullet}C_2C_4$	—	—	—	—
$H^{\bullet}C_3C_2$	50.0	—	69.9	98.2
$H^{\bullet}C_3C_4$	—	—	—	43.0
$H^{\bullet}C_4C_3$	—	—	—	50.2
OC_2C_3	56.6	84.2	99.7	52.0
OC_2C_4	—	—	—	125.0
OC_3C_2	97.8	70.4	54.7	102.6
OC_3C_4	—	—	—	157.7
HOH	104.6	104.4	104.7	104.6

atom from atom C_2 to C_3, but also the cleavage of the C_2–C_3 bond and formation of the C_2–C_4 bond. The migrating hydrogen atom is positioned between atoms C_2 and C_3; the H–C_2 and H–C_3 distances and the HC_2C_3 angle are 116 pm, 157 pm, and 58°, respectively. The C_2–C_3 and C_2–C_4 distances of 183 and 161 pm suggest cleavage of the former and formation of the latter bond. The positive charge appears to be localized mainly in atom C_4 according to the Mulliken charges.

3.2.5. Production of 2,3-DMB-2 (TS7)

A second pathway for the production of 2,3-DMB-2 is through the direct branching rearrangement of species A to F. This reaction proceeds via transition state TS7, whose structure is shown in Fig. 9 while energetic and structural parameters are listed in Tables 2 and 8, respectively. The activation energies for the forward and reverse reactions are predicted to be 94 and 99 kJ/mol, respectively. TS7 resembles a protonated cyclopropane ring, with the migrating hydrogen atom positioned between C_3 and C_4. The forward reaction also requires the cleavage of the C_2–C_3 bond and formation of the C_2–C_4 bond. The C_2–C_4 distance of 157 pm indicates the formation of this bond. The positive charge appears to be localized in atom C_2 according to the Mulliken charges.

The optimized structure of the transition state for the direct branching rearrangement in the presence of water (TS7–W) is shown in Fig. 7, and the corresponding energetic and structural parameters are listed in Tables 4 and 9. The activation energies for the forward and reverse reactions are 104 and 95 kJ/mol, respectively, which are higher than the experimental value of approximately 73 kJ/mol reported by Brouwer and coworkers (13, 14). Nevertheless, our predictions are within the error expected from DFT calculations. The activation energy for the forward reaction is 10 kJ/mol higher than that predicted in the gas phase, since the tertiary cation A is stabilized by water more than TS7. In particular, the magnitudes of the energy changes upon interaction with water are 53 and 42 kJ/mol for species A and TS7, respectively (Table 4).

The branching rearrangement of species A to F in the presence of a water molecule involves a separation of charge within TS7–W, as indicated by Mulliken population analyses (Figs. 3 and 7). The charge localized in the hydrocarbon fragment of TS7–W is 98% of the total charge, compared to 60% for species A and F in the presence of

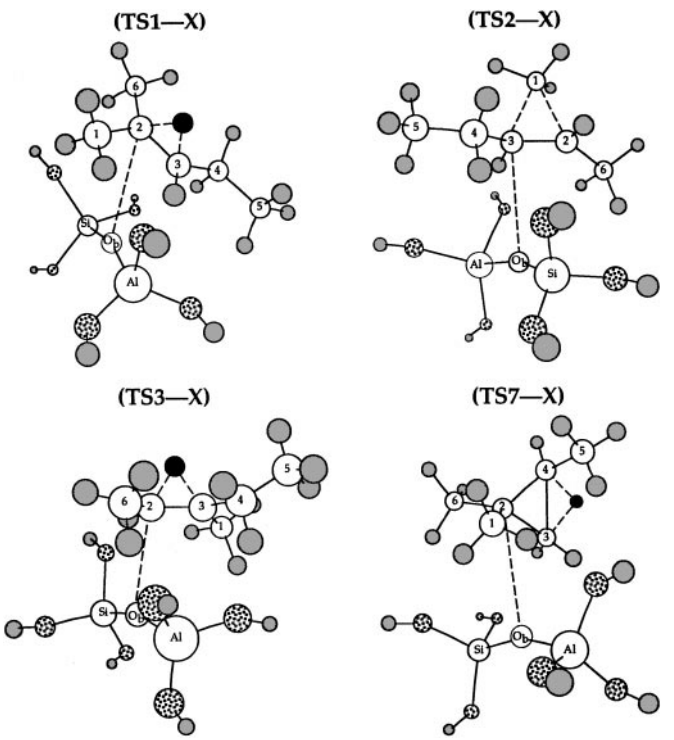

FIG. 8. Transition states for the elementary reactions (TS1-X) A-X ↔ B-X, (TS2-X) B-X ↔ C-X, and (TS7-X) A-X ↔ F-X. The structural parameters are listed in Table 6.

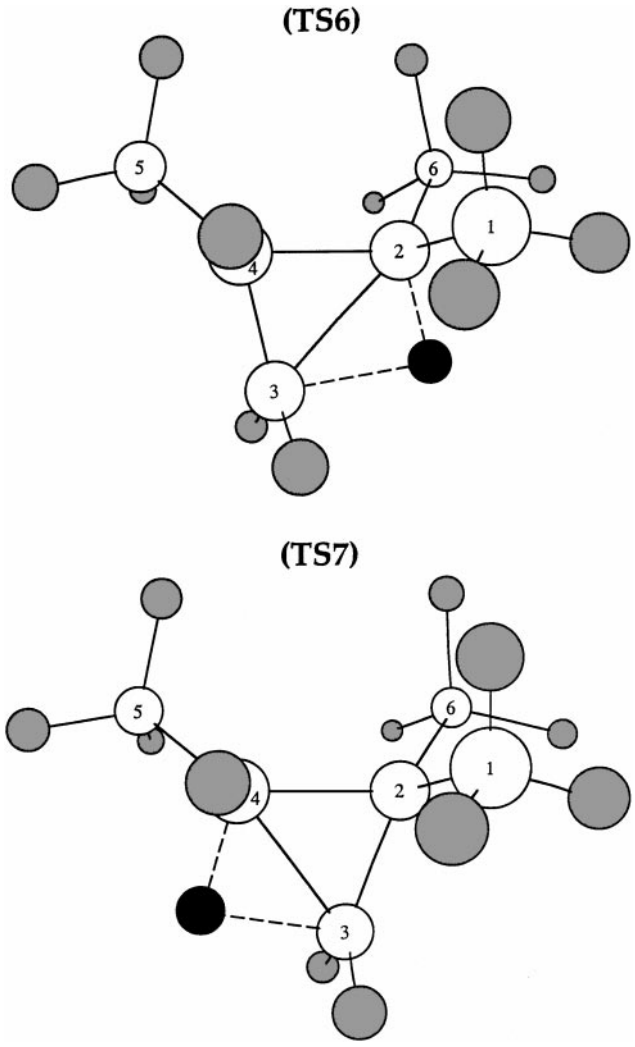

FIG. 9. Transition states of elementary reactions (TS6) E ↔ F and (TS7) A ↔ F. The structural parameters are listed in Table 8.

water. In addition, the C_2–O and C_3–O distances are relatively long (337 and 272 pm, respectively), suggesting that TS7–W consists essentially of a carbenium ion (TS7) and neutral water.

The optimized structure of TS7 interacting with the aluminosilicate cluster is shown is Fig. 8. Structural parameters and reaction energetics are listed in Tables 6 and 7, respectively. The activation energy for the forward (A-X → F-X) reaction is predicted to be 117 kJ/mol relative to gaseous 2-MP-2 plus the acid site. As in the analogous case involving alkoxonium ions, the activation of A-X to produce F-X via branching rearrangements requires the separation of charge, leading to a transition state that resembles a carbenium ion plus the conjugate basic form of the oxide cluster; Mulliken charges for the hydrocarbon fragment within A-X and F-X are $+0.30e$ and $+0.25e$, whereas this charge is increased to $+0.58e$ within TS7-X. The existence of a carbenium ion within TS7-X is also evident from the long C_2–O and C_3–O distances and the predicted rehybridization of these carbon atoms from a sp^3 state in the alkoxy species to a nearly sp^2 state in the transition state.

4. DISCUSSION

The isomerization of gaseous hexyl cations involves branching and nonbranching rearrangements whose rates are significantly different. In particular, nonbranching rearrangements consist of relatively fast 1,2-migrations of hydrogen atoms and methyl groups whose activation energies are predicted to be lower than 30 kJ/mol for species of the same cationic order, or relative to the less stable cation. The energetic difference between reactive intermediates also plays an important role: this difference is 40–50 kJ/mol between secondary and tertiary cations. Transition states for reactions of cations of the same order have the positive charge delocalized within two-electron, three-center bonds involving the migratory entities, which are symmetrically positioned between the cationic centers of the reactants and products. Transition states for reactions of cations of different order resemble the less stable, in our case secondary, cations. On the other hand, branching rearrangements, whose activation energies are predicted to be near 94 kJ/mol, are more complex reactions involving the simultaneous cleavage and formation of C–C and C–H bonds. Transition states for these transformations resemble protonated cyclopropane rings. The complete energy profile for the isomerization of gaseous hexyl cations is shown in Fig. 10.

Activation energies predicted for the isomerization of gaseous hexyl cations are generally higher than those determined experimentally in superacidic solutions by Brouwer and coworkers (13, 14). While uncertainties in these energies can be caused by inaccurate accounting of electron-correlation effects by the DFT method (50–52), these discrepancies could indicate that reaction models based on gaseous carbenium ions are not applicable to studies in condensed media. Better agreement between predicted and experimental activation energies is generally obtained if hexyl cations are allowed to interact with water to form alkoxonium ions. For example, the proper ordering of the rates of 1,2-methyl versus 1,2-hydride shifts is obtained for reaction models based on alkoxonium ions. The complete energy profile for reactions of these alkoxonium ions is shown in Fig. 10. Transformations of alkoxonium ions are less dependent on the degree of the cations since their relative energies are less sensitive to the cationic order. Reactions of alkoxonium ions are determined mainly by the required separation of electronic charge upon activation of the reactive intermediates: ~60% of the total positive charge is localized in the hydrocarbon fragments of alkoxonium ions while this charge is increased to more than 98% of the total charge within transition states. Therefore, since carbenium ions of the same order are stabilized more by

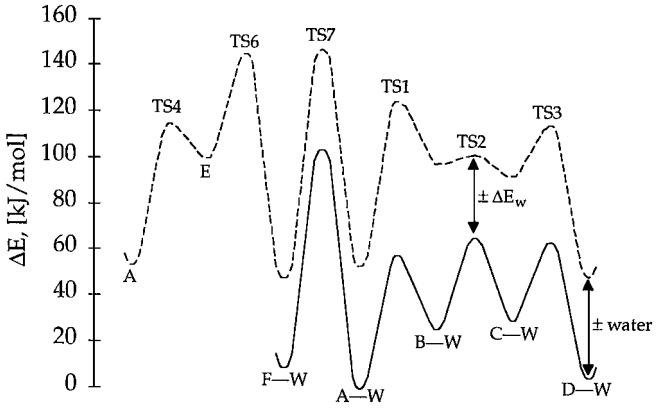

FIG. 10. Energy profile for isomerization of gaseous hexyl cations (dashed line) and cations interacting water (solid line) through nonbranching and branching rearrangements. The energies are reported relative to that of alkoxonium ion A–W.

interactions with water than the corresponding transition states, activation energies are predicted to increase with respect to those for gaseous reactions.

The use of a water molecule in our structural models allows for an understanding of the factors that limit the transformation of hexyl species in the presence of an oxygenated (conjugate) base. However, the deprotonation energy of hydronium ions is too low (706 kJ/mol) compared to that of acidic oxides (1000–1600 kJ/mol) to allow for the generation of a quantitative model of the relevant surface chemistry. Furthermore, reaction intermediates on oxide surfaces are expected to be (neutral) alkoxy species in contrast to (charged) alkoxonium ions. This situation is represented in the present study by calculations involving neutral aluminosilicate clusters having a deprotonation energy of 1420 kJ/mol. The complete energy profile for reactions of these alkoxy species is shown in Fig. 11.

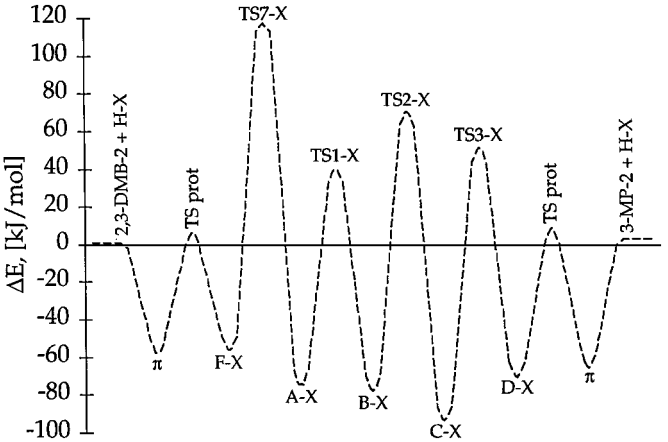

FIG. 11. Energy profile for isomerization of hexyl species on an aluminosilicate site. The energies are reported relative to gaseous 2-MP-2 plus the acid site. Activation energies for the protonation of π-complexes are assumed equal to that calculated for the protonation of 2-MP-2 (Table 7).

The reaction scheme for the isomerization of 2-MP-2 to 4-MP-2, 3-MP-2, and 2,3-DMB-2 over aluminosilicates can be written as

adsorption (desorption)

2-MP-2 + H-X ⇌ 2-MP-2---H-X
4-MP-2 + H-X ⇌ 4-MP-2---H-X
3-MP-2 + H-X ⇌ 3-MP-2---H-X
2,3-DMB-2 + H-X ⇌ 2,3-DMB-2---H-X

protonation (deprotonation)

2-MP-2---H-X ⇌ A-X
4-MP-2---H-X ⇌ B-X
3-MP-2---H-X ⇌ D-X
2,3-DMB-2---H-X ⇌ F-X

isomerization

A-X ⇌ B-X
B-X ⇌ C-X
C-X ⇌ D-X
A-X ⇌ F-X,

where H-X represents the Brønsted acid site.

To compare the results of our calculations with experimental data for isomerization of 2-MP-2 to give 4-MP-2 over aluminosilicate catalysts, it is necessary to derive a rate expression based on the reaction scheme presented above. For this purpose, we make the following assumptions:

(1) adsorption–desorption processes are quasi-equilibrated;

(2) free energies of activation for protonation–deprotonation processes are independent of the nature of the alkene;

(3) free energies of isomerization steps are independent of the nature of alkoxy species such that rate coefficients for the forward and reverse reactions are equal in each step; and

(4) reaction conditions are such that only 4-MP-2 is formed.

On the basis of these assumptions, the overall rate of isomerization ($\Re$) in the limit of zero pressure of 4-MP-2 can be expressed as

$$\Re_{4MP2} = f(\theta, G)\, g(G, PA),$$

where f and g are functions of surface coverage by alkoxy species (θ), Gibbs free energies of gaseous and surface species (G), and the proton affinity of the catalyst site (PA). Specifically,

$$f(\theta, G) = \frac{K_\pi K_p P_r}{1 + (1 + K_p) K_\pi P_r}$$

$$g(G, PA) = \frac{k_{AB}}{1 + 2K_p(k_{AB}/k_p)},$$

where k_{AB} and k_p are rate coefficients for surface isomerization (A-X $\rightarrow$ B-X) and protonation reactions, respectively; K_p and K_π are equilibrium constants for surface protonation reactions and for π-adsorption of 2-MP-2; and P_r is the partial pressure of 2-MP-2. It should now be noted that, since

$$2K_p \frac{k_{AB}}{k_p} \ll 1,$$

the effective rate coefficient for the production of 4-MP-2 is approximately given as

$$k_{4MP2}^{eff} \approx k_{AB} K_\pi K_p = \frac{k_B T}{h} K_{AB}^{\neq} K_\pi K_p,$$

where k_{AB} has been replaced by its estimate from transition state theory (69). The product $K_{AB}^{\neq} K_\pi K_p$ is the overall equilibrium constant for the reaction:

$$\text{2-MP-2} + \text{H-X} \rightleftharpoons \text{TS1-X}.$$

Therefore, the rate of double-bond isomerization is determined by the free energy of the transition state (TS1-X) with respect to gaseous 2-MP-2 plus the acid site, and it is not controlled by the relative stabilities of π or alkoxy complexes.

The dependence of the rate of double-bond isomerization on the acidity of the catalyst is incorporated implicitly in g through activation energies for surface protonation (E_p) and isomerization (E_{AB}) reactions. This dependence on surface acidity becomes evident if one assumes that

$$E_p = E_p^0 - \varepsilon_p$$

$$E_{AB} = E_{AB}^0 - \varepsilon_{AB},$$

where E_p^0 and E_{AB}^0 are defined with respect to the weak-acid limit (e.g., amorphous aluminosilicates) and positive values of ε_p and ε_{AB} correspond to stronger acids, such that

$$\Re_{4MP2} = f(\theta, G) \frac{k_{AB}^0 \exp\left(\frac{\varepsilon_{AB}}{RT}\right)}{1 + 2K_p \frac{k_{AB}^0}{k_p^0} \exp\left(\frac{\varepsilon_{AB} - \varepsilon_p}{RT}\right)}.$$

As discussed later, we expect ε_p to be less sensitive than ε_{AB} to changes in the acid strength of the catalyst; therefore, $\varepsilon_p < \varepsilon_{AB}$, and $\Re_{4MP2}$ increases as the catalyst becomes more acidic.

We now note that McVicker and co-workers (45, 46, 48) measured the overall activation energy to be 23 kJ/mol for the rate of formation of 4-MP-2 from 2-MP-2. According to the analysis presented above, this value should be compared to the energy of TS1-X relative to gaseous 2-MP-2 plus the acid site, which is predicted to be 41 kJ/mol (Table 7). These experimental and predicted values of the overall activation energy are in agreement, in view of the simplistic nature of the aluminosilicate cluster used throughout our studies.

We consider next the rate of production of 3-MP-2 from 2-MP-2. It can be seen in Fig. 11 that the activation energy for the conversion of B-X to C-X is predicted to be higher than for the conversion of A-X to B-X and of C-X to D-X. Therefore, we may assume that

$$k_{AB} \approx k_{CD} \gg k_{BC}.$$

Also, we note that all rate coefficients for surface isomerization reactions are smaller than k_p, since the activation energy for the protonation of 2-MP-2 is low (6 kJ/mol). Application of these assumptions leads to the following expression (in the limit of zero pressure of 4-MP-2 and 3-MP-2):

$$\Re_{3MP2} = K_p \frac{k_{BC}}{k_p} \Re_{4MP2}.$$

In a manner analogous to that discussed above, one can show that the effective rate coefficient for the production of 3-MP-2 is approximately given as

$$k_{3MP2}^{eff} \approx k_{AB} K_\pi K_p^2 \frac{k_{BC}}{k_p} = \frac{k_B T}{h} \frac{K_{AB}^{\neq} K_{BC}^{\neq} K_\pi K_p^2}{K_p^{\neq}},$$

where all rate coefficients have been replaced by their estimates from transition state theory (69). The product $K_{AB}^{\neq} K_{BC}^{\neq} K_\pi K_p^2 / K_p^{\neq}$ is the overall equilibrium constant for the reaction

$$\text{2-MP-2} + \text{H-X} + \text{TS}_p\text{-X}, \rightleftharpoons \text{TS1-X} + \text{TS2-X},$$

where TS_p-X is the transition state for the surface protonation of 2-MP-2. Therefore, the rate of production of 3-MP-2 is determined by the free energy of transition state TS1-X with respect to gaseous 2-MP-2 plus the bare acid site and by the free energy of TS2-X with respect to TS_p-X. The rate of reaction is not affected by the relative stabilities of π or alkoxy complexes.

The ratio of the rate of production of 3-MP-2 to that of 4-MP-2 (selectivity, S_{3MP2}) is approximately given as follows:

$$S_{3MP2} \approx K_p \frac{k_{BC}}{k_p}.$$

The dependence of S_{3MP2} on the surface acidity becomes evident if one assumes that

$$E_p = E_p^0 - \varepsilon_p$$
$$E_{BC} = E_{BC}^0 - \varepsilon_{BC},$$

where E_p^0 and E_{BC}^0 are defined with respect to the weak-acid limit and positive values of ε_p and ε_{BC} correspond to stronger acids, such that

$$S_{3MP2} \approx K_p \frac{k_{BC}^0}{k_p^0} \exp\left(\frac{\varepsilon_{BC} - \varepsilon_p}{RT}\right).$$

As discussed later, surface protonation reactions are expected to be less sensitive than isomerization reactions to changes in the acidity of the catalyst; therefore, $\varepsilon_p < \varepsilon_{BC}$, and S_{3MP2} increases as the catalyst becomes more acidic. This predicted behavior is in agreement with experimental observations (45, 46, 48).

The activation energies for the forward reactions B-X → C-X → D-X involved in the production of 3-MP-2 are predicted to be 71 and 52 kJ/mol, respectively, relative to gaseous 2-MP-2 plus the acid site. These barriers are comparable to the values of 55 and 23 kJ/mol reported by McVicker and coworkers (45, 46, 48) for the 1,2-shifts of methyl groups and hydrogen atoms over amorphous aluminosilicates. Discrepancies between our predictions and experimental values are probably caused by the high deprotonation energy of the simplistic aluminosilicate cluster chosen for our studies.

We consider next the production of 2,3-DMB-2 from 2-MP-2 over aluminosilicate clusters. It can be seen in Fig. 11 that the activation energy for the reaction A-X → F-X is considerably higher than for all other isomerization reactions; therefore, we may assume that

$$k_{AB} \approx k_{CD} \gg k_{BC} \gg k_{AF}.$$

Also, we note that all rate coefficients for surface isomerization reactions are smaller than k_p. On the basis of these assumptions, the following rate expression is obtained (in the limit of zero pressure of products):

$$\Re_{23DMB2} = \frac{k_{AF}}{k_{AB}}\left(1 + K_p \frac{k_{AB}}{k_p}\right)\Re_{4MP2}.$$

The ratio of the rate of production of 2,3-DMB-2 to that of 4-MP-2 (selectivity, S_{23DMB2}) is approximately given as

$$S_{23DMB2} \approx \frac{k_{AF}}{k_{AB}}\left(1 + K_p \frac{k_{AB}}{k_p}\right).$$

The dependence of S_{23DMB2} on the surface acidity becomes evident if one assumes that

$$E_p = E_p^0 - \varepsilon_p$$
$$E_{AB} = E_{AB}^0 - \varepsilon_{AB}$$
$$E_{AF} = E_{AF}^0 - \varepsilon_{AF},$$

where E_p^0, E_{AB}^0, and E_{AF}^0 are defined with respect to the weak-acid limit and positive values of ε_p, ε_{AB}, and ε_{AF} correspond to stronger acids, such that

$$S_{23DMB2} \approx \frac{k_{AF}^0}{k_{AB}^0} \exp\left(\frac{\varepsilon_{AF} - \varepsilon_{AB}}{RT}\right)\left\{1 + K_p \frac{k_{AB}^0}{k_p^0} \exp\left(\frac{\varepsilon_{AB} - \varepsilon_p}{RT}\right)\right\}.$$

The production of 2,3-DMB-2 is favored over stronger acid catalysts if surface branching reactions are more sensitive than 1,2-hydride shifts and surface protonation reactions to changes in the acidity of the catalyst; that is, if $\varepsilon_{AF} > \varepsilon_{AB} > \varepsilon_p$.

An alternative approach to the generation of a rate expression for the rate of branching reactions consists of assuming that π-adsorption and surface protonation processes are quasi-equilibrated in comparison to the branching rearrangement, in view of the high activation energy for this isomerization step. The surface coverage by A-X is then given by

$$\theta_{A-X} = K_\pi K_p P_r \theta_{H-X},$$

and the forward rate of branching is

$$\begin{aligned}\Re_{23DMB2} &= k_{AF}\theta_{A-X} \\ &= k_{AF} K_\pi K_p P_r \theta_{H-X} \\ &= \frac{k_B T}{h} K_{AF}^{\neq} K_\pi K_p P_r \theta_{H-X},\end{aligned}$$

where k_{AF} has been replaced by its estimate from transition state theory (69). The product $K_{AF}^{\neq} K_\pi K_p$ is the overall equilibrium constant for the following reaction:

$$\text{2-MP-2} + \text{H-X} \rightleftharpoons \text{TS7-X}.$$

Therefore, we conclude that the rate of branching rearrangements and, more generally, the rates of alkene isomerization reactions are determined by the free energies of transition states with respect to the gaseous reactants plus the acid site and not by the relative stabilities of π and alkoxy intermediates in the reaction scheme. It is for this reason, and the fact that transition states have a high degree of charge separation, that kinetic models based on carbenium-ion chemistry have been effective for the

description of reactions of hydrocarbons on solid acid catalysts.

Finally, we consider whether our calculations can explain why McVicker and co-workers have found that weak acids catalyze 1,2-hydride shifts in 2-MP-2 to produce 4-MP-2; that stronger acids are required to catalyze methyl migrations that lead to 3-MP-2; and that even stronger acids are needed to achieve branching rearrangements involved in the production of 2,3-DMB-2. We have seen that the rate of production of 4-MP-2 is controlled by the free energy of TS1-X with respect to gaseous 2-MP-2 plus the acid site H-X, and we defined ε_{AB} as the change in the energy of TS1-X with respect to the acidity of the catalyst. We have also shown that the rate of production of 3-MP-2 is controlled by the free energy of TS1-X relative to gaseous 2-MP-2 plus the acid site, and by the free energy of TS2-X relative to that of TS_p-X; ε_{BC} and ε_p were defined as the changes in energy of TS2-X and TS_p-X with respect to the acidity of the catalyst. Moreover, we have shown that the rate of production of 2,3-DMB-2 is controlled by the free energy of TS7-X with respect to gaseous 2-MP-2 plus the acid site, and we defined ε_{AF} as the change in the energy of TS7-X with respect to the acidity of the catalyst. To explain the selectivity trends observed by McVicker and co-workers in terms of acid strength, we need $\varepsilon_{AF} > \varepsilon_{BC} > \varepsilon_{AB} > \varepsilon_p$. This trend is, in fact, justified by the Mulliken charges of 0.58*e*, 0.54*e*, 0.51*e*, and 0.48*e* of the hydrocarbon fragments in TS7-X, TS2-X, TS1-X, and TS_p-X, respectively. Hence, there is a correlation between the charge localized in the hydrocarbon fragment of a transition state in an alkene isomerization scheme and the sensitivity of the corresponding reaction pathway to changes in the acidity of the catalyst. The transition state for branching rearrangement (TS7-X) requires the greatest separation of electronic charge in the aluminosilicate cluster, and its energy is most sensitive (through ε_{AF}) to changes in the acidity of the cluster, that is, the ability of the cluster to donate a proton. The transition state for methyl migration (TS2-X) requires the second greatest separation of electronic charge in the aluminosilicate cluster, and its energy is thus less sensitive (through ε_{BC}) to changes in the acidity of the cluster. Transition states for hydride shifts (TS1-X and TS3-X) require a smaller separation of electronic charge in the aluminosilicate cluster, and their energies are even less dependent (through ε_{AB}) to changes in the acidity of the catalyst. Lastly, the transition state for the protonation of 2-MP-2 (TS_p-X) to form alkoxy species requires the least separation of electronic charge in the aluminosilicate cluster, and the energy of this transition state is expected to be the least sensitive (through ε_p) to changes in the acidity of the cluster. These observations imply that the greater the extent of charge separation in the transition state of certain reaction pathway in an alkene isomerization scheme, the more sensitive is the selectivity for this pathway to changes in the acidity of the catalyst.

5. CONCLUSIONS

The acid-catalyzed conversion of 2-methyl-pentene-2 (2-MP-2) to 4-methyl-pentene-2 (4-MP-2), 3-methyl-pentene-2 (3-MP-2), and 2,3-dimethyl-butene-2 (2,3-DMB-2) has been studied on the basis of density-functional theory. The production of 4-MP-2 and 3-MP-2 can be described as proceeding first through the protonation of 2-MP-2 to form the tertiary 2-methyl-pentyl-2 species. These species can undergo 1,2-hydride migrations and subsequent deprotonation reactions to yield 4-MP-2. Alternatively, they can react via consecutive 1,2-shifts of hydrogen atoms and methyl groups to yield 3-MP-2. The production of 2,3-DMB-2 from 2-MP-2 can be described through initial protonation of 2-MP-2 to form tertiary 2-methyl-pentyl-2 species, which can react via two pathways. One pathway involves a 1,3-hydride shift to form secondary 4-methyl-pentyl-2 species, which can react further via hydride and methyl migrations to yield 4-MP-2 and 3-MP-2, or can undergo branching rearrangement to yield 2,3-DMB-2. The second pathway consists of direct branching rearrangements of tertiary 2-methyl-pentyl-2 species to form tertiary 2,3-dimethyl-butyl-2 species, and thereby yield 2,3-DMB-2.

The activation energies calculated for reactions of gaseous carbenium ions are not in good agreement with experimental results for reactions in superacidic solutions. Better agreement is achieved if the carbenium ions are allowed to react with a conjugate base, such as the oxygen atom of water. Reaction intermediates interacting with oxygenated (conjugate) bases such as water or an aluminosilicate site resemble alkoxonium ions and alkoxy complexes, respectively, and hydrocarbon fragments within the transition states resemble carbenium ions. Transition states for reactions of cations of the same order contain two-electron, three-center bonds involving the migratory entity, whereas transition states for reactions of cations of different order resemble the less stable cation. In the presence of water or on an aluminosilicate site, secondary intermediates are stabilized more than tertiary intermediates, and all intermediates are generally stabilized to a greater extent than transition states. Accordingly, the activation energies associated with reactions involving cations of the same order are increased upon interaction with the oxygenated (conjugate) base. The relative energies of alkoxonium ions and alkoxy species are fairly insensitive to their secondary or tertiary nature. In all cases, isomerization reactions of alkoxonium ions and alkoxy species require the separation of charge within the transition state. The rates of alkene isomerization reactions are determined by the free energies of transition states with respect to the gaseous reactants plus the acid site, and not by the relative stabilities of π and alkoxy intermediates in the reaction scheme.

Finally, our calculations provide an explanation to why McVicker and coworkers found that weak acids catalyze

1,2-hydride shifts in 2-MP-2 to produce 4-MP-2; that stronger acids are required to catalyze methyl migrations leading to 3-MP-2; and that even stronger acids are needed to achieve branching rearrangements involved in the production of 2,3-DMB-2. Specifically, transition states for the protonation of alkenes to form alkoxy species require the least separation of electronic charge in the aluminosilicate cluster; transition states for hydride shifts require a greater separation of electronic charge; the transition state for methyl migration requires an even greater separation of electronic charge; and the transition state for direct branching rearrangements requires the greatest separation of electronic charge in the aluminosilicate cluster. These observations imply the existence of a correlation between the positive charge localized in the hydrocarbon fragment of a transition state and the sensitivity of the corresponding reaction pathway to changes in the acidity of the catalyst.

ACKNOWLEDGMENTS

The authors acknowledge the financial support of the Office of Basic Energy Sciences of the Department of Energy and the National Center for Clean Industrial and Treatment Technologies. We also acknowledge GEM and AOF fellowships awarded to M.A.N.S. and an AOF fellowship awarded to R.A.

REFERENCES

1. Satterfield, C. N., "Heterogeneous Catalysis in Industrial Practice," 2nd ed. McGraw–Hill, New York, 1991.
2. Corma, A., *Chem. Rev.* **95**, 559 (1995).
3. Van Santen, R. A., and Kramer, G. J., *Chem. Rev.* **95**, 637 (1995).
4. Meusinger, J., Vinek, H., and Lercher, J. A., *J. Molec. Catal.* **87**, 263 (1994).
5. Shertukde, P. V., Marcelin, G., Sill, G. A., and Hall, W. K., *J. Catal.* **136**, 446 (1992).
6. Moffat, J. B., *in* "Theoretical Aspects of Heterogeneous Catalysis" (B. Davis, Ed.). Van Nostrand–Reinhold, New York, 1990.
7. Abbot, J., and Wojciechowski, B. W., *J. Catal.* **113**, 353 (1988).
8. Abbot, J., and Wojciechowski, B. W., *J. Catal.* **115**, 1 (1989).
9. Wojciechowski, B. W., and Corma, A., "Catalytic Cracking: Catalysis, Chemistry, and Kinetics." Dekker, New York, 1986.
10. Corma, A., Planelles, J., Sánchez-Marín, J., and Tomás, F., *J. Catal.* **93**, 30 (1985).
11. Corma, A., Planelles, J., and Tomás, F., *J. Catal.* **94**, 445 (1985).
12. Gates, B. C., "Catalytic Chemistry." Wiley, New York, 1992.
13. Brouwer, D. M., and Hogeveen, H., *Progr. Phys. Org. Chem.* **9**, 179 (1972).
14. Brouwer, D. M., *in* "Chemistry and Chemical Engineering of Catalytic Processes" (R. Prins and G. C. A. Schuit, Eds.). Sijthoff & Noordhoff, Alphen aanden Rijn, The Netherlands, 1980.
15. Haw, J. F., and Xu, T., *Adv. Catal.* **42**, 115 (1998).
16. Xu, T., and Haw, J. F., *J. Am. Chem. Soc.* **116**, 7753 (1994).
17. Haw, J. F., Nicholas, J. B., Xu, T., Beck, L. W., and Ferguson, D. B., *Acc. Chem. Res.* **29**, 259 (1996).
18. Stepanov, A. G., Zamaraev, K. I., and Thomas, J. M., *Catal. Lett.* **13**, 407 (1992).
19. Kazansky, V. B., *Acc. Chem. Res.* **24**, 379 (1991).
20. Malkin, V. G., Chesnokov, V. V., Paukshtis, E. A., and Zhidomirov, G. M., *J. Am. Chem. Soc.* **112**, 666 (1990).
21. Haw, J. F., Richardson, B. R., Oshiro, I. S., Lazo, N. D., and Speed, J. A., *J. Am. Chem. Soc.* **111**, 2052 (1989).
22. Aronson, M. T., Gorte, R. J., Farneth, W. E., and White, D., *J. Am. Chem. Soc.* **111**, 840 (1989).
23. Zardkoohi, M., Haw, J. F., and Lunsford, J. H., *J. Am. Chem. Soc.* **109**, 5278 (1987).
24. Bates, S. P., and van Santen, R., *Adv. Catal.* **42**, 1 (1998).
25. Rigby, A. M., Kramer, G. J., and van Santen, R. A., *J. Catal.* **170**, 1 (1997).
26. Frash, M. V., Solkan, V. N., and Kazansky, V. B., *J. Chem. Soc.: Faraday Transactions* **93**, 515 (1997).
27. Natal-Santiago, M. A., de Pablo, J. J., and Dumesic, J. A., *Catal. Lett.* **47**, 119 (1997).
28. Mota, C. J. A., Esteves, P. M., and de Amorim, M. B., *J. Phys. Chem.* **100**, 12418 (1996).
29. Evleth, E. M., Kassab, E., Jessri, H., Allavena, M., Montero, L., and Sierra, L. R., *J. Phys. Chem.* **100**, 11368 (1996).
30. Viruela-Martín, P., Zicovich-Wilson, C. M., and Corma, A., *J. Phys. Chem.* **97**, 13713 (1993).
31. Kazansky, V. B., Sechenya, I. N., and Pankov, A. A., *J. Molec. Catal.* **70**, 189 (1991).
32. Sechenya, I. N., and Kazansky, V. B., *Catal. Lett.* **8**, 317 (1991).
33. Kazanskii, V. B., *Bull. Acad. Sci. USSR: Div. Chem. Sci.* **39**(9), 2058 (1990).
34. Kazansky, V. B., and Sechenya, I. N., *J. Catal.* **119**, 108 (1989).
35. Kazansky, V. B., Frash, M. V., and van Santen, R. A., *Catal. Lett.* **48**, 61 (1997).
36. Blaszkowski, S. R., Nascimento, M. A. C., and van Santen, R. A., *J. Phys. Chem.* **100**, 3463 (1996).
37. Kramer, G. J., and van Santen, R. A., *J. Am. Chem. Soc.* **117**, 1766 (1995).
38. Blaszkowski, S. R., Jansen, A. P. J., Nascimento, M. A. C., and van Santen, R. A., *J. Phys. Chem.* **98**, 12938 (1994).
39. Kramer, G. J., van Santen, R. A., Emeis, C. A., and Nowak, A. K., *Nature* **363**, 529 (1993).
40. Kazansky, V. B., Frash, M. V., and van Santen, R. A., *11th Int. Congr. Catal.* **101**, 1233 (1996).
41. Collins, S. J., and O'Malley, P. J., *Chem. Phys. Lett.* **246**, 555 (1995).
42. Collins, S. J., and O'Malley, P. J., *J. Catal.* **153**, 94 (1995).
43. Kazansky, V. B., Senchenya, I. N., Frash, M. V., and van Santen, R. A., *Catal. Lett.* **27**, 345 (1994).
44. Kazansky, V. B., Frash, M. V., and van Santen, R. A., *Catal. Lett.* **28**, 211 (1994).
45. Kramer, G. M., McVicker, G. B., and Zieman, J. J., *J. Catal.* **92**, 355 (1985).
46. Kramer, G. M., and McVicker, G. B., *Acc. Chem. Res.* **19**, 78 (1986).
47. McVicker, G. B., Kramer, G. M., and Ziemiak, J. J., *J. Catal.* **83**, 286 (1983).
48. Soled, S. L., McVicker, G., Miseo, S., Gates, W., and Baumgartner, J., *11th Int. Congr. Catal.* **101**, 563 (1996).
49. Carbó, S., Planelles, J., Ortí, E., Viruela, P., and Tomás, F., *J. Mol. Struc. (Theochem)* **150**, 33 (1987).
50. Sieber, S., Buzek, P., Schleyer, P. v. R., Koch, W., and de M. Carneiro, J. W., *J. Am. Chem. Soc.* **115**, 259 (1993).
51. Boronat, M., Viruela, P., and Corma, A., *J. Phys. Chem.* **100**, 633 (1996).
52. Boronat, M., Viruela, P., and Corma, A., *J. Phys. Chem.* **100**, 16514 (1996).
53. Becke, A. D., *J. Chem. Phys.* **98**, 5648 (1993).
54. Hehre, W. J., Radom, L., and Schleyer, P. v. R., "Ab Initio Molecular Orbital Theory." Wiley, New York, 1986.
55. Davidson, E. R., *Int. J. Quant. Chem.* **69**, 241 (1998).
56. Kohn, W., Becke, A. D., and Parr, R. G., *J. Phys. Chem.* **100**, 12974 (1996).
57. Ziegler, T., *Chem. Rev.* **91**, 651 (1991).

58. Frisch, M. J., Trucks, G. W., Schlegel, H. B., Gill, P. M. W., Johnson, B. G., Robb, M. A., Cheeseman, J. R., Keith, T., Petersson, G. A., Montgomery, J. A., Raghavachari, K., Al-Laham, M. A., Zakrzewski, V. G., Ortiz, J. V., Foresman, J. B., Cioslowski, J., Stefanov, B. B., Nanayakkara, A., Challacombe, M., Peng, C. Y., Ayala, P. Y., Chen, W., Wong, M. W., Andres, J. L., Replogle, E. S., Gomperts, R., Martin, R. L., Fox, D. J., Binkley, J. S., Defrees, D. J., Baker, J., Stewart, J. P., Head-Gordon, M., Gonzalez, C., and Pople, J. A., "Gaussian 94 (Revision C.2)." Gaussian, Inc., Pittsburgh, PA, 1995.
59. Peng, C., Ayala, P. Y., Schlegel, H. B., and Frisch, M. J., *J. Comp. Chem.* **17**(1), 49 (1996).
60. Peng, C., and Schlegel, H. B., *Israel J. Chem.* **33**, 449 (1993).
61. González, C., and Schlegel, H. B., *J. Chem. Phys.* **90**(4), 2154 (1989).
62. González, C., and Schlegel, H. B., *J. Phys. Chem.* **94**, 5523 (1990).
63. Levine, I. N., "Quantum Chemistry." Prentice–Hall, Englewood Cliffs, NJ, 1991.
64. "Gas Phase Ion Chemistry" (M. T. Bowers, Ed.), Vol. 2. Academic Press, New York, 1979.
65. Sauer, J., Ugliengo, P., Garrone, E., and Saunders, V. R., *Chem. Rev.* **94**, 2095 (1994).
66. Kramer, G. J., and van Santen, R. A., *J. Am. Chem. Soc.* **115**, 2887 (1993).
67. Sauer, J., *Chem. Rev.* **89**, 199 (1989).
68. Zhidomirov, G. M., and Kazansky, V. B., *Adv. Catal.* **34**, 131 (1986).
69. Laidler, K. J., "Chemical Kinetics," 3rd ed. HarperCollins, New York, 1987.